UNIVERSITÀ DEGLI STUDI DI CATANIA
FACOLTÀ DI SCIENZE MATEMATICHE, FISICHE E NATURALI
DOTTORATO DI RICERCA IN FISICA

ELISA BRUGALETTA

ROTATIONAL EVOLUTION

BETWEEN 120 MYR AND 1 GYR

PH.D. THESIS

Supervisor:
Prof. A. C. Lanzafame

Coordinator:
Prof. F. Riggi

XXVI CICLO (2010-2013)

Abstract

In this work the rotational evolution and the lithium depletion of low -mass stars in young stellar system is investigated, taking advantage of extensive new data sets on rotational periods that have recently became available. The rotational evolution of slow-rotating stars between 100Myr and 1 Gyr have been examined in detail, outlining a complex behaviour that claim for improved modelling of the internal angular momentum transport and of the angular momentum loss via a magnetised wind. A puzzling change in the rotation distribution vs. mass takes place at 550 Myr, which seems to contradict current theoretical models. Previous assumptions on the factorisation of the rotational dependence on time and mass do not hold in the 100 Myr - 1 Gyr time interval, which complicates somewhat the age inference from rotation. Studies based on the distribution of rotational periods of solar-type stars suggest in addition a possible link between lithium depletion and the rotational history of stars. The dispersion of lithium abundance at a given color in the Pleiades member stars have been re-examined. Once removed the mass dependence from rotation and Li-depletion a soft correlation between lithium and rotational periods in K and M type stars has been found. On the other hand, a clear and solid correlation has been found in the $0.74 \leq (B-V) < 1.15$ color range. In this (B-V) range the slower a star is the larger is the lithium depletion. A comparison and an analysis of the rotation periods and lithium depletion in young stellar association AB Doradus and the Pleiades has allowed to confirm the coevality for these two systems. A group of slow-rotating stars in AB Dor, however, have Li abundance considerably higher that suggested by the general trend, which may be indicative of differences in the rotational histories of stars belonging to the young loose association. A young nearby cluster, $\gamma^2 Velorum$, has also been analyzed, using data from the Gaia-ESO survey. This latter has evidenced the presence of two possible different populations. These populations are kinematically different eventual differences in Li abundance are found below detectability.

Contents

Introduction

Age, mass and chemical composition are the fundamental attributes of stars. The age of stars are estimated through models or empirical methods, and no single method works well for a broad range of stellar types or for a large range in age (see Soderblom (2010) for a review of the general problem). Coeval stellar systems, like clusters and associations, are of outermost importance in deriving methods for inferring stellar ages.

As discussed by Barnes (2007), rotation provides an attractive alternative chronometer because changes steadily and it is function of age and color. However, the theory of angular momentum evolution is really complex because is the result of an interplay between initial conditions during star formation, the evolution of stellar structure and the behaviour of stellar winds and magnetic fields. The simplest model available for computing stellar wind torques begins with the distribution of rotation rates in protostars and evolves them forward assuming solid body rotation and a scaled solar angular momentum loss rate $dJ/dt \backsimeq \omega^3$ (Kawaler (1988)). This model reproduces the Skumanich (1972) law $P \propto \sqrt{t}$. Since the angular momentum loss depends on rotation, the large spread in rotation present in very young systems converges to a narrow mass-rotation relationship at a given age by the age of the Hyades.

Barnes (2007) suggested that the influence of color (mass) and age are independent effects on rotational period evolution, thus mathematically a simple product of two separable functions ($P((B-V),t) = f(B-V) \times g(t)$). A few variations of the Barnes' relation exist but none reproduces in a satisfactory way the new data available for the Pleiades (Hartman et al. (2010)). For the purposes of this work a new calibration of the period-mass-age relationship has been done from the Pleiades' age (120 Myr) to NGC6811's age (1 Gyr). The factorisation $P = f(B-V)g(t)$, however, cannot describe the empirical rotational evolution in this age range. Ro-

tation, in fact, evolves differently at different mass and therefore it has been necessary to discard the possibility of a factorisation, modifying the *g(t)* function in a $g = g(B-V,t)$ function. A further complication arises, however, since the evolution is found to change in an unexpected fashion after 550 Myr. A thorough assessment of the consequences of this behaviour for the validity of current models of the angular momentum evolution require further investigation.

Like rotation, lithium is an extraordinarily sensitive diagnostic of stellar structure and evolution. The observed lithium abundances in stars reveal an extreemely complex picture. As initially observed by Danziger et al. (1966) Pleiades stars exhibit spreads in lithium abundance. Since this phenomenum is so closely correlated with rotation (that is capable of driving an extra mixing, as first noticed by Pinsonneault et al. (1989)) it is necessary to discuss lithium in the context of the rotation observations. For this reason the dispersion in Li abundance in the Pleiades has been analysed relating it to the period-mass relationship derived in this work. The analysis has outlined an almost uniform correlation between Li abundance and rotation in the $0.74 \leq (B-V) \leq 1.15$ colour range, as opposed to a simply systematic difference between ultra-fast rotators and all other stars found by previous authors.

In this context the analysis of the young loose association AB Doradus adds some other useful information in the rotational evolution of low-mass stars. Availing of the results obtained for the Pleiades for rotational period and its correlation with lithium depletion, a comparison has been done to corroborate or not the Luhman et al. (2005) hypothesis that AB Dor and the Pleiades have common origin despite the different environment (UV, winds, encounters). The comparison of the period distribution in the two systems show that these have the same rotational ages. The distribution of Li abundance are very similar, but a small group of stars may indicate somewhat different rotation and Li-depletion histories for the two stellar systems.

Finally, being a member of the GAIA-ESO Survey gave me the opportunity to work with new data obtained for the young nearby cluster $\gamma^2 Velorum$ (5-10 Myr, 350 pc) using the FLAMES/GIRAFFE spectrograph on the VLT. For this cluster, stellar parameters have been derived including Li-abundance. A preliminary analysis of two sub-populations discovered in the contest of this investigation is presented.

This thesis summarizes the result of the work performed during my three years

of PhD and is structured in the following way:

- Chapter 1: some relevant information on the theory of rotational period and lithium abundance evolution are introduced;
- Chapter 2: the whole dataset used for the analysis is described;
- Chapter 3: the empirical description of the rotation-mass-age evolution from 120 Myr to 1 Gyr is presented;
- Chapter 4: the Pleiades lithium depletion analysis and its correlation with the rotational period is presented;
- Chapter 5: the possibility to support the common origin of AB Doradus and the Pleiades availing of the relationships found for the Pleiades is discussed;
- Chapter 6: the results of preliminary analysis on the new data acquired for the cluster $\gamma^2 Velorum$ are presented;
- Chapter 7: conclusions are presented.

Chapter 1

Rotational evolution and lithium depletion of low-mass stars

Fundamental stellar properties such as mass, radius and rotation can be derived through basic observables such as orbital motion, eclipses and period measurements. In contrast stellar ages have no firm basis and are critical to establish. When an age indicator is constructed there are about five steps that need to be considered:

- it's necessary to find an observable, v, that changes sensitively and smoothly, it's better if monotonically, with age. Preferably this observable would be a property of the individual star rather than that of a coeval collection of them.
- One needs to determine the ages of calibrating objects independently, otherwise systematic errors will be introduced.
- It's necessary identify the functional form of the variable: $v = v(t, w, x, \ldots)$, where t is the age and w,x,... are other possible additional dependencies of the variable. It's obviously preferable to have fewer variables and to have separable dependencies of the form $v = T(t) \times W(w) \times X(x) \ldots$
- One needs to invert the dependence determined to find $t = t(v, w, x, \ldots)$
- Finally, one needs to calculate the error $\delta t = \delta t(t, v, w, x, \ldots)$

Recent progress has been made on the quantitative estimation of ages for stars of roughly solar-mass and solar-metallicity that are younger than the Sun. Methods for estimating stellar ages include:

- *Hertzsprung-Russell diagram*, one can estimate the age of cluster by identifing exactly what type of star is undergoing the transition from Main Sequence to red giant (called the Main Sequence Turn-Off), and knowing how long (theoretically) that it takes stars of that type to use up all of their hydrogen;

- *Chromospheric activity*: the flux of the chromospheric emission core of the H and K lines of the Ca II normalized to the bolometric emission of the star, $R'_{HK} = (L_{HK}/L_{bol})$, is a function of time;
- *Coronal activity*: $R'_{xray} = (L_{xray}/L_{bol})$ is a function of age;
- *Asteroseismology*: the detection of oscillation modes in stars is an indicator of the stars' central density, which is a function of age;
- *Rotation*: it decreases with time due to loss of angular momentum with stellar wind;
- *Lithium*: the depletion of light elements is related to standard stellar evolution, Li being particularly useful because easy to observe and its changes with age are large.

This thesis examines aspects related to the determination of age using rotation, related to the stellar evolution, and Li-depletion, also related to stellar evolution with an important role played by the rotational history. The presence of a strong absorption in the $LiI\lambda6708\mathring{A}$ line indicative of a young age despite generally there is a spread at constant age and mass. On solar-type stars photosphere obvious manifestations of magnetic activity are the dark star-spots (active regions) which move across the disk, and the energetic flares which are typically associated with them. Spots are a common features in young, active solar-type stars; observations in open clusters show that the G and K dwarfs often exhibit strong *rotational modulation* in their light curves. Photometric rotational modulation is attributed to the presence of these starspots rotating in and out of view, and is distinguished by its periodicity (the rotation period of the star) and smoothly varying, often sinusoidal, shape. Of all the activity-related properties of stars rotation is the most fundamental and together with stellar mass it might be responsible, directly or indirectly, for the observed morphology of all the other activity indicators. Fig. 1.1 shows an example of photometric light curves for solar-type dwarfs from a survey of young stellar associations (Messina et al. (2010)).

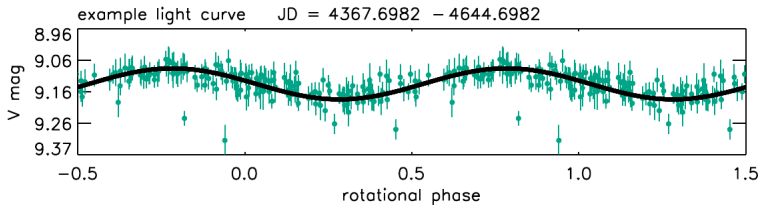

Figure 1.1: Light curves of a member of Carina association. TYC 9390 0322 1 it's a K0V star showing photometric modulation typical of starspots rotating across the stellar surface. The derived period is $P = 1.858d$ and the solid line is a sinusoidal fit.

1.1 Rotational evolution

The evolution of stellar angular momentum is one of the most problematic issue in the early formation and accretion history of a star. It is known from the beginning that a young star must carry angular momentum and cross spin-up and spin-down phases during its life. For this reason, rotation period measurements in open clusters and young associations give one of the most stringent information on the angular momentum evolution of late-type stars. Rotation is an important ingredient of the dynamo process and can influence the surface abundance of light elements through rotationally induced mixing and it's also related to the formation and evolution of planetary systems. Rotation changes depend on both the evolution of the internal structure (stellar radius contraction during the pre main sequence and its expansion during post main sequence) and on the presence and evolution of intense magnetic fields that are significantly related to stellar mass.

Historically a real interest in rotational properties of pre-main sequence stars was kicked off with the discovery that many T Tauri stars rotate much slower than predicted by the theory (Herbig (1962)). T Tauri stars represent the initial hydrostatic evolutionary stage for stars, and rotation measurements in star forming regions therefore set the initial conditions for angular momentum evolution. During the PMS T-Tauri phase solar mass stars undergo a global contraction and the magnetic fields are responsible for the star-disk coupling that keeps the stars's rotation rate slow (this phase lasts to $\sim 5 - 10Myr$). The circumstellar discs that surround these stars in the earliest stages of their evolution have the effect to remove angular momentum holding the angular velocity of the star almost constant for its lifetime. The disc lifetime's range is expected to produce a spread of rotation rates on the PMS and ZAMS. During the MS and post MS the magnetic fields are responsible for the angular momentum loss by means of magnetized stellar winds.

Evolution of angular momentum and magnetic activity offer complementary diagnostics to study the mechanisms by which rotation and magnetic fields influence each other. It is necessary to invoke two mechanisms of angular momentum removal: one operating for $\sim 5-10 Myr$ on the PMS and one operating on the main sequence, with the property that it must produce a convergence in the rotation rates between ~ 100 and $600 Myr$. Fig. 1.2 summarize this scenario, showing calculate rotational tracks from Schulz (2005).

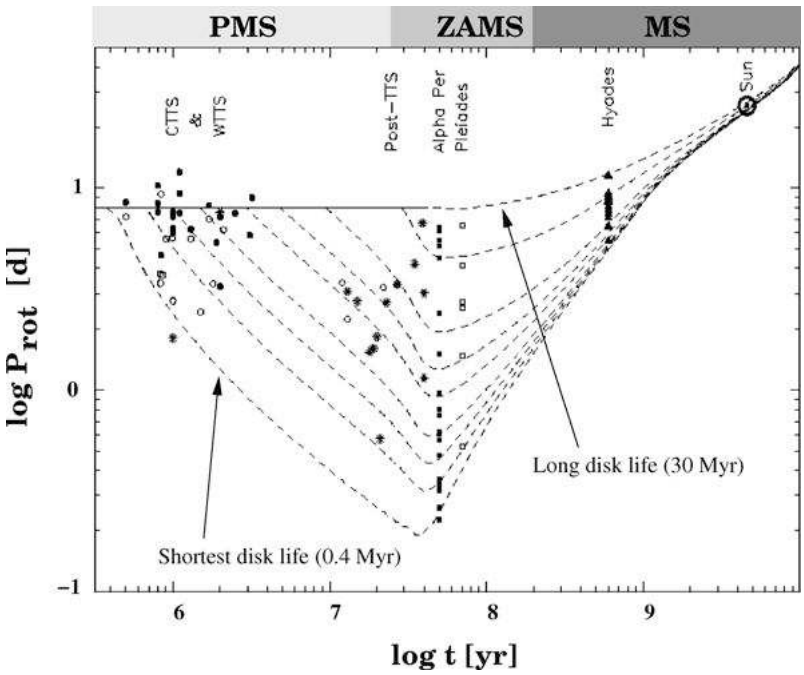

Figure 1.2: The evolution of rotational periods of young solar-mass stars towards the Sun's period on the MS. The lowest dashed curve relates to short disk lifetimes, the top curve to very long disk lifetimes (Schulz (2005)).

In recent years, photometric measurements of stellar rotation periods, based on the rotational modulation of the light curve induced by photospheric inhomogeneities that can be either cool or hot spots arising from magnetic activity, have replaced the measurements based on the $v \sin i$ as derived from spectral line profiles. This has considerably improved both the number and the precision of available rotational periods. The observed variability is dominated by phenomena that are manifested on different timescales. The shortest timescale, of the order of seconds to minutes, is related to micro-flaring activity. The varibility on timescales from several hours to days is mostly related to star's rotation. The variability on timescale from months to years is related to the growth and decay of active regions and the presence of starspot cycles (like the $\sim 11 yr$ sunspot cycle). Surface period measurements become an indirect probe of the internal rotation profile of these stars if it

is assumed that the radiative core and the convective envelope rotate rigidly at all ages with a differential rotation between them, e.g. Spada et al. (2011) and reference therein. This difference could be parameterized through a coupling time-scale, τ_c, which determines the rate of angular momentum exchange between the two regions. Open clusters and star forming regions have been crucial for developing the standard picture of angular momentum evolution in low mass stars. Stars in open clusters provide snapshots in time of the evolution of stellar rotation. Stars of the same mass are born with a range of rotation and early models predicted that stars in open clusters would converge to a narrow mass-rotation relationship at fixed age, but did not correctly predict the existence of either the most rapid or the slowest rotating stars in the young ones. These initial variations in the rotation rates of young stars, that become increasingly unimportant with the passage of time, converge onto a single well-defined relationship. This relationship depends to first order only on the mass and age of the star and permits the determination of rotational ages with a technique called "gyrochronology" (Barnes (2003)). Gyrochronology relationships are typically calibrated to cluster data in the color range $0.5 \lesssim (B-V)_0 \lesssim 1.4$. The interest in modeling the structure and the evolutionary tracks of very low-mass stars have recently grown because these rappresent a large fraction of stellar population.

The timescale that determines the convergence onto the rotation-mass relationship can be long, especially in lower mass dwarfs. This timescale is important because the median rotation-mass-age relationship only becomes a good chronometer after stars have forgotten their initial conditions. The reddest stars in the cluster exhibit a large dispersion in rotation rate at young ages. As observed by Epstein et al. (2012), also when the scatter of rotational periods from the relationship is not small, the rotation rates still encode statistical information abount ages, also if the rotation-age solution is not unique. Indeed, until stars loose the memory of their initial conditions, one cannot distinguish between an inactive young star and an active older star at the same rotation period. This implies that must be taken into account a minimum error in the mean rotation-mass-age relationship due to the intrinsic dispersion in the stellar rotation rates.

Observations have clearly demonstrated that once a low-mass star (G and later) reaches the main sequence it begins to lose angular momentum; this is understood to be the result of a magnetized stellar wind. By comparing the rotation velocities of stars in the Pleiades and the Hyades with the Sun, Skumanich (1972) found the

scaling relation that relates the avaraged surface rotational velocities, $vsini$, of stars to their ages, t, via the expression

$$v \sin i \propto 1/\sqrt{t} \tag{1.1}$$

A theoretical model that can explains this behaviour is that made by Kawaler (1988). This model predicts that surface angular momentum loss rate is proportional to the cube of angular velocity, or ω^3. Naturally it leads to a convergence in the rotation rates of stars. The presence of solar-mass rapid rotators appears to contradict the Skumanich law and suggests that the angular momentum loss rate is saturated above some critical rotation rate ω_{crit}. The critical rotation rate must be mass dependent to explain the spread in rotation rates for lower mass stars. The rotation history of a star will depend not only on the rate of angular momentum loss, but also on the efficiency of internal angular momentum transport.

In their pioneering study on stellar rotation among main-sequence stars in the Hyades open cluster Radick et al. (1987) found a correlation between the (B-V) colours and the rotation periods of F, G and K stars. This study remained unparalleled for nearly two decades after its publication since the advent of wide-field surveys for exoplanetary transit in open clusters using small instruments (like 1-m class telescopes). The first empirical calibration of stellar spin rates as a function of age and colour was published by Barnes (2003).

1.2 The I and C sequence

In his work Barnes (2003) plotted together, ranking by age (from 30 Myr for the youngest open clusters to ∼4.5 Gyr), the measured rotation periods against dereddened (B-V) color (Fig. 1.3). The rotation periods of open clusters stars appear not to sample a single population, with a possibly wide dispersion that varies with stellar mass and age. Instead, there is evidence for subpopulations in these color-period diagrams. He named these the I and C sequences and called the cuneiform region between them *gap*. The fraction of stars in this gap (to the total number of stars in the cluster) is relatively high at 30-50 Myr and steadily decreases. The gap, despite the name, is not empty and contains a comparable, if smaller, number of stars to that on the C sequence. The presence of stars in the gap suggests that some stars jump off the C sequence and migrate to the I sequence. The low density of stars in the gap region for all the clusters indicates that stars spend less time in this part of the diagram than on the C and I sequences.

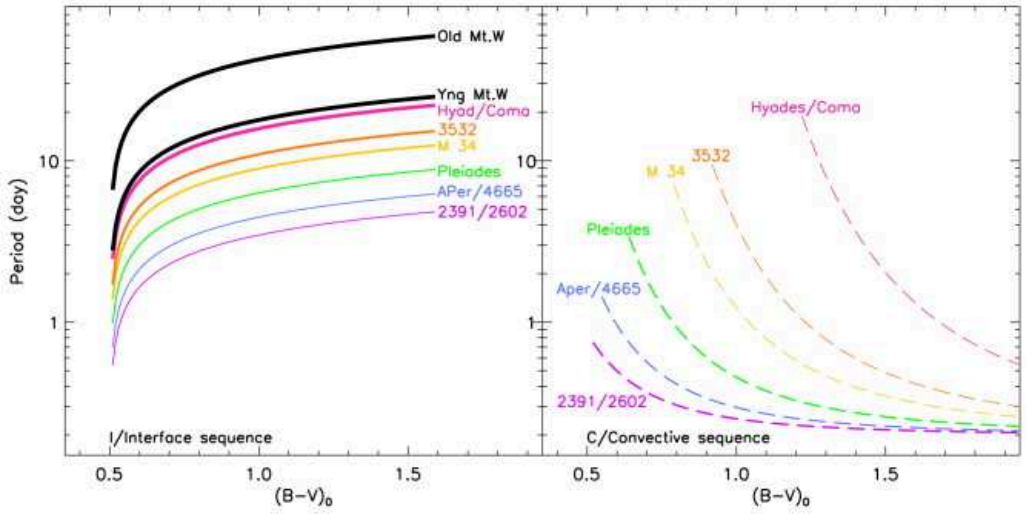

Figure 1.3: Schematic curves, from the parameterizations of Barnes (2003), representing the variation from cluster to cluster of the I (left) and C (right) sequence. The thickness of each line represents the fraction of stars in the sequence. IC2391 and IC2601 30 Myr, Alpha Per and IC4665 50Myr, Pleiades 100Myr, NGC3532 300Myr, Hyades and Coma 600Myrs, Young Mt. Wilson 800Myr, Old Mt. Wilson 4.5 Gyr.

1.2.1 The I sequence

The slow/interface/I-sequence consists of stars that form a diagonal band of increasing period with increasing (B-V) color. It is only faintly visible in the youngest open clusters, 30-50 Myr, and becomes clearly visible by 200 Myr accounting an increasingly fraction of stars with increasing cluster age. The positive slope of the I-sequence increases systematically with stellar age. Stars with spectral type late-F (bluer than $(B-V) = 0.5$) have higher mass that do not have surface convection zones and do not easily spin down. The sequence was suggested by Barnes (2003) to be associated with the existence of a radiative/convective interface and for this reason was also called *radiative sequence*. The I sequence in open clusters spins down approximately Skumanich style (Eq. (1.1)). These facts suggested Barnes that it might be possible to account for both the color dependence and time dependece of rotation to attempt the construction of rotational isochrones for late-type stars. The particular functional form chosen, so as to incorporate the Skumanich relationship and separate the mass (f(B-V) instead of f(M) only for observational convenience) and age (g(t)) dependencies, is:

$$P(t, B-V) = g(t) \times f(B-V)$$

where

$$g(t) = \sqrt{t}$$

$$f(B-V) = \sqrt{(B-V-0.5)} - 0.115(B-V-0.5)$$

P, t, and (B-V) are respectively the rotation period (days), age (Myr) and (B-V) color. Few years later he re-calibrated this curve and determined a new form for these functions (Barnes (2007)):

$$g(t) = t^{0.5189 \pm 0.0070} \tag{1.2}$$

$$f(B-V) = (0.7725 \pm 0.011)((B-V) - 0.4)^{0.601 \pm 0.024} \tag{1.3}$$

1.2.2 The C sequence

The sequence of fast rotators (UFRs) is also observed, bifurcating away from the I-sequence toward shorter rotation periods. The fast/convective/C sequence, initially well populated, becomes increasingly sparse with cluster age. The observed increasing fraction of stars on the I-sequence and the coupled diminishing fraction on the C-sequence imply that stars evolve steadily from the C-sequence to the I-sequence. The motion of the bifurcation point between the sequences suggests that the timescale of this evolution is zero for F-type stars and increases toward 300 Myr for M-type stars. The color dependence of the C-sequence is the reverse of that of stars on the I-sequence, and bluer stars spin down faster. This fact suggests that the material involved in this spin-down is not that of the entire star but only that of the surface convection zone since the extent of the convection zone has the opposite color dependence than the mass of the entire star. The surface convection zone for stars on the C-sequence is substantially decoupled from the inner radiative zone. For I-sequence stars apparently have a different magnetic field and the convective and radiative zone are connected. The fact that the C-sequence does not cross or extend past the I-sequence suggests that the C field changes to the I field, or becomes dominated by it, on a timescale that varies from zero for F stars to $\sim 200 - 300 Myr$ for K-M stars. Stars in the gap could be interpreted as those that are switching or have switched magnetic configuration from C to I type.

1.3 Lithium role in stellar evolution understanding

Lithium is important for the understanding of a wide range of astrophysical processes ranging in scale from the stellar to the cosmological. Various Galactic processes can create and destroy it, and thus tracing the evolution of lithium in Galaxy can illuminate these processes and, more generally, Galactic chemical evolution. Both due to its cosmological interest and because it is regarded as a good indicator of the

pre-main sequence history of stars what is learned in one field can influence another.

The relatively low temperature at which lithium is destroyed makes it quite easily damaged and so a crucial diagnostic of the physical processes occurring in stellar interiors. Low mass stars burn both deuterium and lithium during pre-main sequence evolutionary stages (Hillenbrand (2009)), in fully convective stars light elements are depleted troughout the star and the photospheric abundance is a reliable indicator of the interior abundance. The results of observations can be summarized saying that the behaviour of contracting objects is closely related to their mass:

- when $1.25M_{\odot} \lesssim M \lesssim 2.5M_{\odot}$ lithium burning processes are active for only a few tens of Myr to $< 1Myr$, these stars do not experience any strong pre-MS Li-depletion;
- when $M \lesssim 1M_{\odot}$ and down to the hydrogen burning limit stars deplete their lithium essentially forever;
- brown dwarfs burn only deuterium but never lithium.

Lithium depletion trends, in young pre-main sequence and main sequence populations, have been used at sub-solar masses to estimate stellar age. During the pre-main sequence phase stellar temperatures rise to values at which light elements burning begins to occur. Lithium is a good indicator of the pre-MS history of these stars because ^7Li is easily destroyed via the reaction $^7Li(p,\alpha)^4He$ starting at $T \sim 2.5 \cdot 10^6 K$, first at the centre of the star and then, if the temperature is large enough, also at the base of the convective envelope. If this occurs, any physical process that can transport surface material to regions where lithium burning is possible will deplete the observable surface abundance. This extablishes a relationship between the inward extension of the envelope and the amount of ^7Li left at the surface. However, lithium equivalent widths and the derived abundances at constant mass or spectral type are observed to have a significant dispersion in many clusters while other elements are very uniform. This dispersion in surface abundance is likely related to the dispersion in rotation speeds over the same age range. Nonetheless, for any given star, lithium depletion is monotonically related to stellar age. Since stars retain chemical imprints from their formation, they can serve as effective "snapshots" of the composition of the interstellar medium from which they form. Understanding the way in which the surface composition is changed over a star's lifetime is crucial in the interpretation of stellar abundances as they pertain

to Galactic chemical evolution.

In standard stellar theory (SST) (Bodenheimer (1965), Dantona et al. (1984), D'Antona et al. (2003)) the different Li-depletion observed in stars with different masses is explained by the mixing of stellar surface material limited to the surface convective zone (SCZ). If the SCZ does not extend to depths reaching the lithium burning temperature, the lithium surface abundance should not change over time. Significant lithium depletion can occur only during a star's pre-MS evolution because solar-type and cooler stars are fully convective during their initial stages of contraction and transition to a radiative core during their pre-MS lifetimes. Temperatures at the base of the SCZ (the core of the star when fully convective) are too low for lithium burning at the start of the pre-MS but quickly rise above the lithium burning point (within $\sim 2Myr$ for our Sun). The total amount of lithium depletion is dependent on the rate of stellar contraction and formation of a radiative core, which are largely dependent on stellar mass and composition. Stars with higher mass and lower opacity (lower metallicity) will transit more rapidly to a radiative core and impede lithium depletion. Models predict that the depletion in a star is a unique function of age, mass and metallicity allowing larger depletion in lower mass stars which, beeing cooler, have deeper envelopes. The presence of additional physical processes (like overshooting [1]) which mix the surface matter with deeper and hotter layers have obviously a strong impact on Li-depletion.

Historically theoretical research on Li-depletion is connected with the following, still unsolved, problems:

1. the large observed solar Li-depletion, as compared to other solar-type stars.

2. the spread in Li-abundance observed at the end of the pre-MS in young open clusters, at least for masses $M < 1.1M_{\odot}$.

No theoretical model until the work of Ventura et al. (1998) was able to reproduce the large drop in the ^7Li abundance from the initial value of $logN(^7Li) \sim 3.3$ found in the solar system to the current solar value of $logN(^7Li)_{\odot} = 1.16 \pm 0.1$. With

[1] Overshooting is a physical process that occurs in stars when heat is transported by convection. When bouyancy forces vanish, the eddy acceleration vanishes but not the velocity which allows eddies to "overshoot" into the adjacent radiative regions. It brings material with bigger mean molecular weight from the core into regions of lower mean molecular weight.

a 15% decrease in the metallicity $Z_{\odot}$ adopted for the Sun they bring the solar Li-abundance to the observed value. The evidence that for stars in a young open cluster of the same temperature the lithium abundances can vary by factors of up 100 or more was explained considering small inhomogeneties in the star formation regions. This explanation might at least partially answer for the large ^7Li abundance spread which is observed in low mass stars belonging to young open clusters.

1.4 Lithium depletion spread in low-mass stars

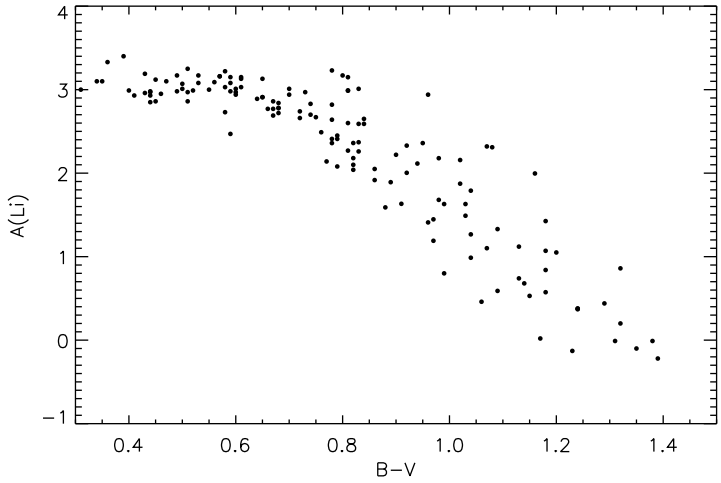

Figure 1.4: Li abundances vs. (B-V) measures in the Pleiades cluster (Sestito et al. (2005)). It's evident the well-known declining trend of Li abundance with increasing color index. Li abundances were computed from T_{eff} and deblended EW from the line at 6707.441$\mathring{A}$ that is believed to be due primarily to Fe I.

Ever since the discovery of the large dispersion of lithium in the Pleiades (Fig. 1.4) it has been supposed that the variation from star to star in the Li content could be caused by convective depletion possibly regulated by the effects of rotation (Danziger et al. (1966)). Butler et al. (1987) looked at a few Pleiades K dwarfs and noted that the Li-rich stars appeared to be the rapid rotators. These ultrafast rotators (UFRs)-Zero-Age Main-Sequence stars rotate at up to 100 times the solar rate. They used the Li abundance as an indicator of relative stellar ages and argued that this correlation between Li abundance and rotation substantiated an age spread within the Pleiades. The slow rotators were thought to be somewhat older than the UFRs as a result of the UFRs losing angular momentum to evolve into stars with more normal rotation rates.

Later works (Duncan (1993) and Soderblom et al. (1993a)) showed that only a

fraction of stars are born with enough angular momentum to become UFRs. Consequently the slow rotators in the Pleiades are not the immediate descendants of UFRs. The existence of real spreads in rotation rates and lithium abundances among group of stars of about the same age emphasized how poorly is understanded those phenomena that are so central to the evolution of solar-type stars.

Soderblom et al. (1993b) reported measurements of lithium in more 100 Pleiads F, G and K dwarfs. They concluded that spots or any inhomogeneous atmosphere can only account for the discordant Li equivalent widths in a superficial sense and that a full consideration of all the available information makes that explanation unlikely. The spread seen in $\log N(Li)$ is unlikely to be due to any agents that influence Li line formation, it is real and large in the Pleiades for $M \lesssim 0.9 M_{\odot}$. They analyzed two extrinsic motivations:

1. variations in the initial Li abundances of stars,

2. a large spread in age within the Pleiades.

Both explanations appeared unsatisfactory. They did not found basis for claiming gross inhomogeneities in the material from which the stars of the cluster have formed, especially since those stars appear to have the same abundances of heavy elements. But the strongest evidence against either of these hypoteses was that stars should have Li abundance variations that are independet of mass. Stars at $1 M_{\odot}$ should be just as affected as stars at 0.9 or $0.7 M_{\odot}$, yet that was not seen. Stars with $M \lesssim 1.1 M_{\odot}$ deplete Li on their way to the ZAMS at a rate that depends primarily in the mass (dN_{Li}/dt increases with decreasing mass and this dependence argues that there is something about stars themselves that causes some to have much more lithium than others) and rotation also play a role helping a star to preserve more of its initial Li.

After Soderblom et al. (1993b) also Xiong et al. (2006) analyzed the stellar activity in the low temperature Pleiades stars and found that is generally understimated. Evidences demonstrate that there are frequent flare star-like activites in the atmospheres of the young active stars which possibly cause the abnormal ionization and excitation of the Li atoms. Also, despite the mechanisms of their action on the abundance anomaly is not understood, various signs indicate that they make an important contribution to the Li abundance dispersion. Stellar activities (including spot activity) change the color and the equivalent width of spectral line. Variations

of the star's luminosity and color produce variations of the apparent magnitude and apparent color index, causing variations in the apparent effective temperature, and apparent Li abundance. Their conclusion was that abnormal ionization and excitation produced by star's surface activities result in variations in the equivalent width of the spectral line $LiI\lambda 6708\mathring{A}$ producing variations in the apparent Li abundance. For this reason, at least a considerable part of the observed Li dispersion is caused by observational effects. The dispersion of Li abundances so may be a spurious dispersion arising from an incomplete analysis rather than a real lithium dispersion in the cluster. However, a recent work made by King et al. (2010) reinforced Soderblom et al. (1993b) hypothesis. From their analysis they noticed that the scatter in KI resonance line (whose condition of formation is very similar to that of LiI) exists, also if it is much less than the scatter in LiI. Their conclusion is that there is evidence for a real dispersion in abundance at fixed effective temperature.

The latest addition of rotation-related physics in stellar models are still unable to account for the large scatter in lithium abundances. Attempts have also been made to relate the lithium dispersion with stellar activity, which is driven by stellar rotation because most of the apparent Li dispersion is caused by the atmospheric effect of active stars. The correlation with stellar rotation is so a reflection of the correlation between the Li abundance and the activity. This finding has been taken as a powerful support to the rotation induction mixing mechanism. Rotational mixing extends trough stellar envelopes, and as a result it can simultaneously mix different elements and be present in stars with very different surface convective zone depths. In this way could be explained the lithium depletion observed in all low mass open cluster stars, which would not be expected if lithium depletion were a phenomenon confined to the convective zone boundary (Pinsonneault (2010)).

Chapter 2

The data-set

Stars form within giant molecular clouds ($10^5 - 10^6 M_\odot$ with a space diameter of 40 pc or more) that become unstable to fragmentation and subsequent gravitational collapse to produce: stellar clusters, multiple star systems and individual stars. A category of young system includes the *open clusters* that are so-called because their individual members can often be clearly distinguished (Stahler et al. (2005), Janes et al. (1988)). An open cluster is a group of stars (from 10 to 10^3) that were formed from the same giant molecular cloud and have roughly the same age. To qualify as a genuine open cluster a group of stars needs to be physically related (Archinal et al. (2003)). The observed density should be sufficiently large as to render the group fairly stable, this stable density is one solar mass per cubic parsec or greater. More than 1,100 open cluster have been discovered within the Milky Way Galaxy. Stars in clusters are loosely bound to each other by mutual gravitational attraction this fact leads dinamically the open clusters gradually to "evaporate". The theory suggests that the main culprint is encounters with giant molecular clouds. The rate of such encounters is low but the cloud mass is so huge that the effect can be devastating. Both molecular clouds and clusters have similar random motions, so their typical relative velocity exceeds a cluster's *internal* velocity. Stars that are closest to the passing cloud respond most strongly and often only a single encounter with a giant molecular cloud is sufficient to disrupt a cluster entirely. Open clusters generally survive for a few hundred million years (half of them reach ages of $10^8 yr$, while about 10% survive as long as $10^9 yr$) and been found only in spiral and irregular galaxies, strongly concentrated toward the galaxy plane, in which active star formation is occurring. The long-term internal evolution of an open cluster is described in terms of energy equipartition from kinetic theory of collisional systems.

Open cluster are key objects in the study of stellar evolution. In contrast to field stars, stars in open cluster form samples that have a wide range of mass and homogeneuous in environmental conditions, initial chemical composition, age and interstellar reddening. Each cluster provides a snapshot of stellar evolution. Thus, observations of many clusters at different ages and chemical compositions, quantify stellar evolution, allowing increasingly datailed theoretical models to be tested that could explain always better the dependence on age and metallicity of different stellar properties and their mutual relationship. Stars in clusters and young association have been studied profusely so it has not been too hard to find the data used for this work. The sample used includes 9 clusters with different ages and an association (listed in table 2.1).

Table 2.1: Name, estimated ages and number of stars used in this work.

Object name	Age (Myr)	stars	Reference
Pleiades	120	241	Hartman et al. (2010)
AB Doradus	120	31	Messina et al. (2010)
M35	150	421	Meibom et al. (2009)
M34	240	118	Meibom et al. (2011)
M11	230	36	Messina et al. (2010)
M37	550	372	Hartman et al. (2009)
Hyades	600	56	Delorme et al. (2010)
Praesepe	600	35	Delorme et al. (2010)
Coma Berenices	600	27	Collier Cameron et al. (2009)
NGC6811	1000	71	Meibom et al. (2011)

For the present analysis were considered stars with $0.5 \leq B - V \leq 1.4$ ranging spectral type from early G to early M with $4000 \lesssim T_{eff} \lesssim 6000K$, the ages range from $\sim 120Myr$ for Pleiades to $\sim 1Gyr$ for NGC6811. The upper limit for the age is related to the variability that become too small to be detectable from the ground. While instrumental and observational errors may be removed by longer baseline monitoring or higher precision photometry, the fact that stars don't have a unique surface rotation period presents an irreducible uncertainty. The solar rotation rate is significantly faster at the equator than near the poles. Because one cannot know if is measuring equatorial rotation rates for unresolved stars, this sets bounds on the precision of rotation period. The rotation period distribution used are extracted from photometric survey of stellar open cluster and young associations, as available in the literature (see columns 4 of table 2.1 for the references). The assumptions for cluster ages are collection of independent determinations, they were

derived by different authors and using disparate models. Thus the dataset is not homogeneous as far as ages are concerned. The classical methods for estimating the age of a cluster, the fit of the turn off or of the low main sequence, are affected by uncertainties mainly due to physical inputs adopted in models. The ages reported are the most recent literaure estimates. Also from the point of view of the data quality the complete set cannot be considered homogeneous; homogeneity would imply that all the stars in all clusters should have been re-observed with an unique instrument. Regardless I felt confident of this dataset because stars in young clusters have been studied extensively by more than one author (in these cases I selected the more recent observations which have a better signal-to-noise ratio and/or higher resolving power in the case of spectroscopic data for the Lithium abundance) and are relatively close, as a result the targets have accurate characterisations.

2.1 Clusters younger than 500 Myr

2.1.1 Pleiades

Figure 2.1: Open cluster Pleiades. With a long exposure from a dark location the dust cloud surrounding the Pleiades star cluster becomes very evident. (picture took from http://apod.nasa.gov/apod/astropix.html)

The Pleiades (Fig. 2.1), or Seven Sisters, is an open cluster containing middle-aged hot B-type stars located in the constellation of Taurus. It is among the nearest star clusters to Earth with a distance $d \sim 133pc$ (Soderblom et al. (2005)). The cluster is dominated by hot blue and extremely luminous stars. Dust that forms a faint reflection nebulosity around the brightest stars is known to be an unrelated dust cloud, recent observations of interstellar gas in the vicinity of the Pleiades

suggests that the cluster is coincidentally colliding with two small molecular clouds moving, relative to Pleiades, at $\sim 15 - 20 kms^{-1}$. However, the mass of the gas is only $20 - 50 M_{\odot}$, which is much smaller than the mass of the cluster stars (Adams et al. (2001)). The cluster core radius is about 8 light years and tidal radius is about 43 light years. It contains over 1,000 statistically confirmed members. The total mass contained in the cluster is estimated to be about 800 solar masses including a 15% correction for unresolved binaries. The cluster contains many brown dwarfs, which are objects with less than about 8% of the Sun's mass, not heavy enough for nuclear fusion reaction to start in their cores and become proper stars. They may constitute up to 25% of the total population of the cluster, although they contribute less than 2% of the total mass. Brown dwarfs contribute little to the dynamical mass. Stars with mass $1 - 0.1 M_{\odot}$ dominate the total mass. Due to its proximity, richness and age, the Pleiade star cluster ($d \sim 133 pc$, age $\sim 120 Myr$, e.g. Stauffer et al. (1998)) has served for many years as one of the benchmark clusters in studies of stellar angular momentum evolution.

In this work a large sample of photometric rotation period for FGK Pleiades stars done by Hartman et al. (2010) has been used. Observations were acquired by the Hungarian-made Automated Telescope Network (HATNet), a project that uses a network of six small-aperture (11cm diameter), wide-field (8×8 deg), fully automated telescope to search for transiting exoplanets orbiting bright stars, to characterize them and also to find and follow bright variable stars. Hartman et al. (2010) presented new rotation period measurements for 368 stars in the Pleiades, increasing by a factor of 5 the number of stars in this cluster with measured periods. The sample is ~ 93 per cent complete for stars with $0.7 \lesssim M \lesssim 1.0 M_{\odot}$. This data-set includes 241 stars, some among the recent compilation of probable Pleiades members by Stauffer et al. (2007) and other new members found by Hartman et al. (2010), that aren't in a binary sistem and for which they give both period measures, B, V, K color index (taken from 2MASS catalogue), mass and radius (estimated from the K magnitude and the Yi et al. (2001) isochrones). Among these for 102 stars are available also a measure of lithium abundance (Sestito et al. (2005) whose main original source is Soderblom et al. (1993b)) computed from T_{eff} (computed from dereddened B-V colors using the calibration $T_{eff} = 1808(B-V)_0^2 - 6103(B-V)_0 + 8899K$) and deblended Li I feature from the line at $6707.441 \mathring{A}$ that is believed to be due primarily to Fe I.

2.1.2 AB Doradus

A Young Loose stellar association is a very loose star cluster, whose stars share a common origin, but have become gravitationally unbound and are still moving together through space. Associations are primarily identified by their common movement vectors and ages. Identification by chemical composition is also used to factor in association memberships. AB Doradus has a mean distance of $\sim 34pc$ (Torres et al. (2008)). The All Sky Automated Survey (ASAS) is the major source of photometric observations on wich Messina et al. (2010) analysis is based. Informations for the few stars that are not in the ASAS database were found using ADS (Astrophysical Data System). The AB Dor Association has 25 known visual binaries (two are triples and one is quadruple), there are also in the AB Dor Association two triple line spectroscopic multiples, three single line spectroscopic binaries and three stars are possible spectroscopic binaries. The data-set includes 31 stars for which are available rotational periods and B-V mag (from ADS, Astrophysical Data System), among these for 28 stars there's also measured the effective temperature (derived from the $(V-I)$ color index) and lithium informations (abundances and equivalent width) (da Silva et al. (2009)).

2.1.3 M35 and M34

All data concerning M34 and M35 clusters have been taken from Meibom et al. (2009) and Meibom et al. (2011). Meibom et al. (2009) data on M35 have been taken in an extensive time-series photometric survey for membership and binarity for late-type stars in the field of the open cluster. M35 is a rich ($\gtrsim 2500$ stars) northern hemisphere cluster located $\sim 800-900pc$ toward the galactic anticenter. It has an age estimate of $150Myr$, based on the isochrone method. The photometric data were obtained in the Johnson V-band with the WIYN $0.9m$ telescope at Kitt Peak. The field of view of this instrument is $20'.5 \times 20'.5$. The large number of observing nights (over 143) and the sampling frequency allowed them to detect photometric variability with periods ranging from less than a day to about 10 days. The data-set includes 421 stars for which they gave rotational periods, V mag, B-V and V-I color index. Meibom et al. (2009) provided also a flag to distinguish between fast, slow rotators and the stars in the gap region. Stars located in the color-period diagram between the lines represented by $P_{rot} = 10(B-V)_0 - 2.5 \pm 2.0$ and with periods above 1.5 days were flagged as slow rotators. Stars redder than $(B-V)_0 = 0.6$ and with periods between 0 and 1.5 days were flagged as fast rotators. Stars located

below $P_{rot} = 10(B-V)_0 - 4.5$ and with periods above 1.5 days were flagged as gap stars. These selection criteria are subjective. However, due to the large number of rotation periods in M35, the small number of stars with uncertain gap/slow rotator identification using slightly different criteria, this will not influence the relative fractions.

Meibom et al. (2011) phtometric data on M34 have been obtained in the Johnson V-band with the same telescope used for M35 (Meibom et al. (2009)). M34 is a northern hemisphere cluster located $\sim 470pc$ toward the galactic anti-center with an average age of $240Myr$ (derived from rotational isochrone) and a metallicity close to solar $[Fe/H] \sim 0.07 \pm 0.04$. The time-series photometry were obtained over a time-span of 143 days for a $40' \times 40'$ region centered on the open cluster M34. The sample allowed them to detect photometric variability with periods ranging from less than a day to about 10 days deriving rotation periods and B-V color index for 118 stars. For both the cluster the authors identify and select the members that belong to the two sequences. The sequence of rapidly rotators ($P_{rot} \lesssim 1$day) and that forms the rich diagonal band of stars whose periods are increasing with increasing color index (decreasing mass).

2.1.4 M11

M11 (NGC6705) is a $\sim 230Myr$ intermediate-age open cluster at a distance of nearly $d = 2.0kpc$. As found by Sung et al. (1999) it's one of the most condensed open clusters in the sky, contains an estimated 2900 stars about 500 of which are brighter than mag 14, within an estimated radius of 16 arcmin. The cluster is subjected to substantial reddening $E(B-V) = 0.428mag$ because of low galactic latitude ($b = -2.8°$). The study made by Messina et al. (2010) is based on observations taken in June 2004 with the 1.0 m telescope at the Mt. Lemmon Optical Astronomy Observatory (LOAO) in Arizona (USA). M11 has a very rich stellar background and it's a very difficult task to identify the cluster members, infact they detected about 33400 stars finding 75 new periodic variables centered on it. Among these only 36 are confirmed members and not eclipsing binary systems. These periodic members have $(B-V)_0 < 1.0$, wich corresponds to main sequence stars of spectral type earlier than K3/4.

2.2 Clusters older than 500 Myr

2.2.1 M37

M37 is an open cluster with an age of $550 \pm 30 Myr$, a reddening of $E(B-V) = 0.227 \pm 0.038 mag$, a distance modulus of $(m-M)_V = 11.57 \pm 0.13$ and a metallicity of $[M/H] = +0.045 \pm 0.044$. In the course of a 20 night survey for transiting planets in the rich open cluster M37 Hartman et al. (2009) have measured the rotation periods of 575 stars with masses $0.2 M_\odot \lesssim M \lesssim 1.3 M_\odot$. The observations consisted of both $g\ r\ i$ photometry for $\sim 16,000$ stars and r time-series photometry for $\sim 23,000$ stars obtained with the Megacam mosaic imager on the 6.5m MMT. The selection left 575 variables stars that are candidate cluster members. They calculated the periods using 3 different algorithms. In this way they produced a clean sample of 372 stars for which periods determined do not differ by more than 10%. B V photometry for this stars is available from Kalirai et al. (2001).

2.2.2 Hyades and Praesepe

As two of the rich, intermediate-age $600 Myr$ open cluster closest to the Hearth (respectively $46 pc$ and $180 pc$), the Hyades and Praesepe provide a vital calibration points for many types of stellar evolution study. Delorme et al. (2010) determined stellar rotation rates using data from the SuperWASP camera array located at the Observatorio del Roque de los Muchachos on La Palma, Canary Island. With its 8 cameras, SuperWASP has a total field of view of $640 deg^2$. They made a cross-identification to find B and V photometry from the litterature (matched with NOMAD and Hipparcos data providing high signal to noise photometry). The data-set includes 56 stars with Hyades membership probabilities greater than 0.5 and 35 in Praesepe cluster.

2.2.3 Coma Berenices

The Coma cluster is a small but nearby star cluster, it is the second closest open cluster to the Sun, lying at a distance of $89.9 \pm 2.1 pc$ with an age of $600 Myr$. Collier Cameron et al. (2009) presented the results of a photometric survey of rotation rates in the Coma Berenices open cluster using data obtained as part of the SuperWASP exoplanetary transit-search programme. They identified 1613 rotational variables in the vicinity of the cluster and then determined which among them are likely to be cluster members. At the end there are 27 stars with membership probabilities greater than 0.5 that have rotation periods measured and B, V photometry avaible.

2.2.4 NGC6811

The Kepler Cluster Study is a program to identify members of the four open clusters within the *Kepler* field of view and to obtain and analyze the light curves to measure stellar rotation periods and search for transiting planets. As member Meibom et al. (2011) studied it. Located near Cygnus and Lyra its color-magnitude diagram (CMD) is highly contaminated with field stars. For this cluster, the author estimated 1 Gyr for the age. This age is based on the recento photometric study made by Mills et al. (2005) whofound and age of 975 Myr, and on an estimate of the cluster age of $1.1 \pm 0.2 Gyr$ based on the color difference between the main-sequence turnoff and the red giant clump (Janes et al. (2011)). The data-set includes 71 stars with rotation periods measurements, g and r colors. B-V color has been obtained tranforming g-r using equations by Jester et al. (2005) corrected by $E_{(B-V)} = 0.1$.

Chapter 3

Rotational evolution up to 1 Gyr

As explained better in Chap. 1, of all the activity-related properties of stars, rotation is undoubtedly the most fundamental and the one we can measure to the greatest precision, and together with stellar mass it might be responsible, directly or indirectly, for the observed morphology of all the other activity indicators (X-ray and chromospheric emission and light element abundances depend on rotation). Besides being obviously independent on the distance, stellar rotation is now known to vary with regularity on the main sequence. Stellar rotation is an initial value problem, and the initial conditions are set by the details of the star formation process. The angular momentum distribution is subsequently modified by angular momentum loss (via star-disk interactions), internal angular momentum transport and angular momentum loss via a magnetized wind. If a coupling between protostars and their accretion disk exists, the initial spread of rotation rates can be amplified and stars can reach the main sequence as relatively slow rotators. The lifetime of accretion disks and their degree of coupling to the parent star is crucial to establishing the rotation on the ZAMS. Regarding the angular momentum transport, assuming that the radiative core and the convective envelope rotate rigidly at all ages, models have successfully reproduced the observations provided a certain amount of differential rotation between the core and the envelope is allowed. This is parameterized through a coupling time-scale τ_c. Observations of clusters with ages $\sim 50-600 Myr$ are essential for constraining this time-scale of coupling between stellar convective and radiative zones. Surface period measurements are so an indirect probe of the internal rotation profile of these stars.

3.1 Re-calibration rotational isochrones using the Pleiades

As introduced in Sect. 1.2, the work of Barnes improves the possibility of using the rotational sequence in the color-period plane to measure the age of a stellar population, much like the sequence in the color-magnitude diagram (CMD). The method of gyrochronology relies on fitting the I-sequence rotational isochrone, with age as a free prameter, to populations of cluster stars or to individual field stars in the color-period plane. As noticed already by Mamajek et al. (2008) the Barnes (2007) relationship does not reproduce Hyades observation predicting rotation periods 50% longer than those found. Since the Pleiades is a well known cluster in Fig. 3.1 are overplotted the curve derived by Barnes (2007) and the cluster's data obtained by Hartman et al. (2010).

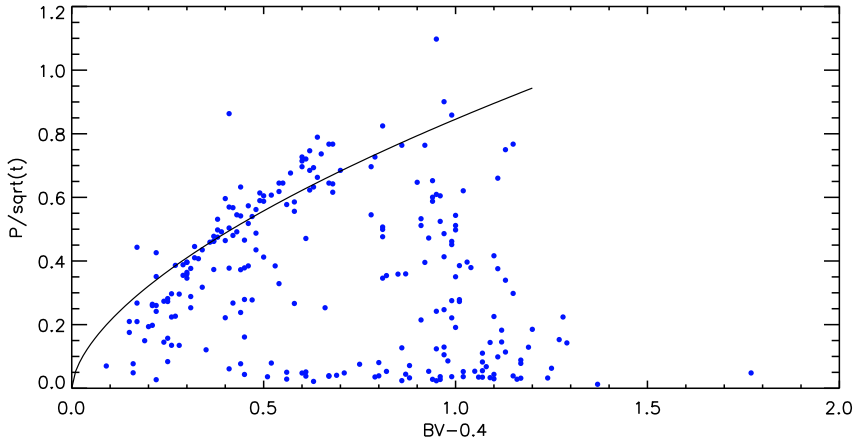

Figure 3.1: Plot of rotation periods vs. (BV-0.4) in the Pleiades. Periods are scaled to the square root of age (120Myr). The periods of stars in the Hartman et al. (2010) data-set are represented. The Barnes's relationship is shown as solid line.

The discrepancy between the Barnes' gyrochrone relationship and the observed period distributions for this benchmark cluster motivated a new determination of the parameters. The slow rotators sequence in the B-V color is quite well defined, from ~ 0.5 to 1.15 (at the beginning of the M-dwarf regime where stars become entirely convective), forming a rich diagonal band of stars whose periods are increasing with increasing color index (decreasing mass). At the blue end of this color range stars have rotation periods of $\sim 1.58d$ while at the red end stars have rotation period of $\sim 8.64d$. Notice that the sequence ends at $T_{eff} \simeq 4000K$ $(B-V \simeq 1.2)$as expected.

For the Pleiades, stars with $(B-V) \leq 1.2$ have already reached the main sequence whereas cooler stars are still on the pre-main sequence (Bell et al. (2012)).

Since, as seen before in the Sect. 1.1, the Skumanich relationship (Eq.1.1) encapsulates something fundamental about the nature of winds and angular momentum loss from late-type stars, it was decided to keep the period dependence on the square root of age. The new fit will concern only the mass-dependence of rotation through the color index B-V with the Barnes' functional form:

$$P/\sqrt{t} = a[(B-V) - b]^c \tag{3.1}$$

In a log-log diagram the function expressed by Eq. (3.1) becomes a straight line so the first step has been to fix the variable b to an initial value of 0.5 and do a linear fit of the eye-selected stars with an idl routine, `LADFIT`, that uses a "robust" least absolute deviation method that attempts to find a function which closely approximates a set of data. It minimizes the sum of the absolute values of the vertical "residuals" between points generated by the function and corresponding points in the data. Least absolute deviations is robust in that it is resistant to outliers in the data (Press et al. (2007)). The results of this preliminary fit is shown in Fig. 3.2.

This preliminary fit still shows some deviation from the trend suggested by the data. A more refined fit was therefore attempted using the original quantities. The idl routine `CURVEFIT` has been applied two times narrowing each time the sample to values within 2σ. This routine computes a non-linear least squares fit to a user-supplied function with an arbitrary number of parameters, the user-supplied function may be any non-linear function where the partial derivatives are known or can be approximated. This method is the Gradient-expansion algorithm which combines the best features of the gradient search with the method of linearizing the fitting function. This is adapted from Marquardt (1963). The final result is shown in Fig. 3.3 and the final functional form is

$$P/\sqrt{t} = (1.111 \pm 0.020)(B-V-(0.476 \pm 0.020))^{0.729 \pm 0.053} \tag{3.2}$$

After the work of Barnes (2007), other authors calibrated the relationship between rotation, color and age using data of several young open cluster. The comparison between three published gyrochronology relationships and the parameters found here is reported in the Table 3.1.

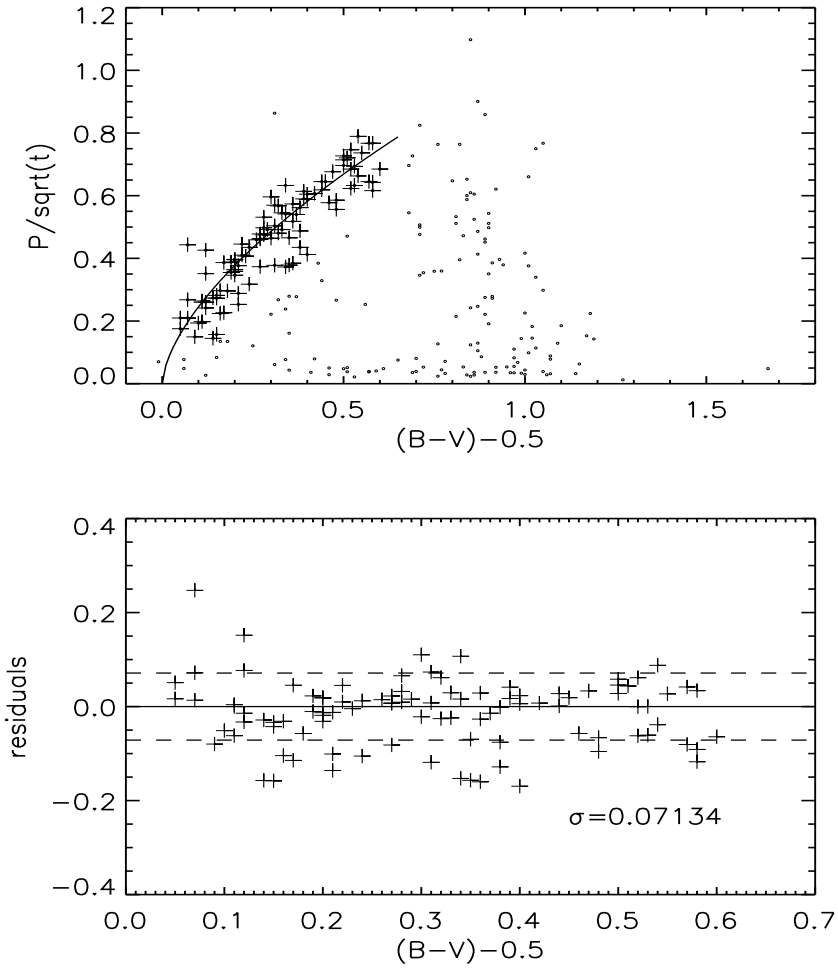

Figure 3.2: On the top with the cross symbol the stars eye-selected and the relation found after the preliminary linear fit on a log-log diagram using `LADFIT`. On the bottom the residuals and the standard deviation of the data set.

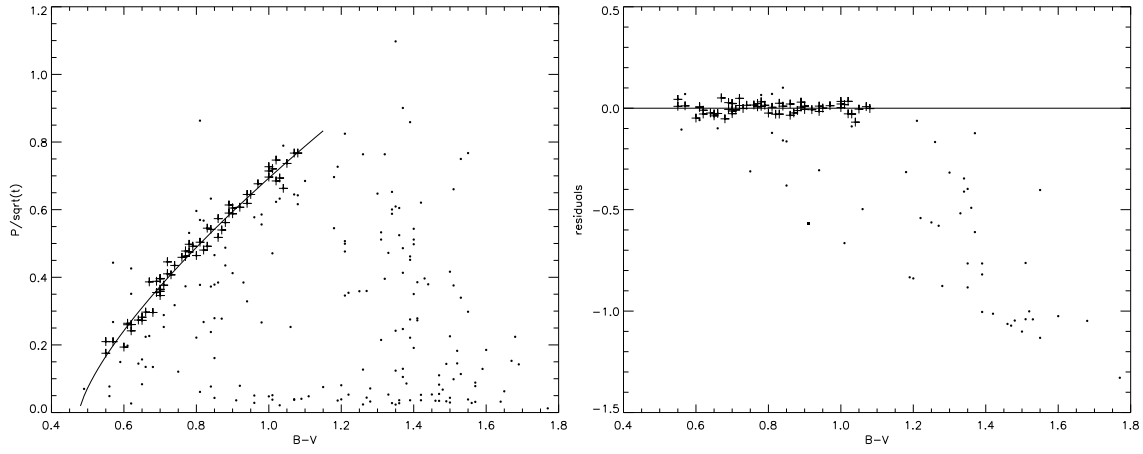

Figure 3.3: Rotation periods vs. (B-V) in the Pleiades. Periods are scaled to the square root of age (in Myr). In the left panel the periods of stars identified with the Barnes I-sequence are marked with the cross symbol and used for the final fit. The fit performed by `CURVEFIT` is shown as solid line. In the right panel the residuals from the fit are shown.

Table 3.1: Function coefficients derived in this work compared with those found by Barnes (2007), Mamajek et al. (2008) and Meibom et al. (2009). n is the age's exponential.

	This work		Barnes et al.		Mamajek et al.		Meibom et al.	
Coefficient	value	σ	value	σ	value	σ	value	σ
a	1.111	0.020	0.7725	0.011	0.407	0.021	0.770	0.005
b	0.476	0.020	0.4		0.495	0.010	0.553	0.0052
c	0.729	0.053	0.601	0.024	0.325	0.024	0.472	0.027
n	0.5		0.5189	0.0070	0.566	0.008	0.52	

These gyrochronology relationships are typically calibrated to cluster data in the color range $0.5 \lesssim (B-V) \lesssim 1.4$. Both Barnes (2007) and Mamajek et al. (2008) based the color-rotation relationship on many well studied clusters (as αPer, Pleiades, Hyades, etc.). Meibom et al. (2009) fit the color dependence in a single cluster (M35). The b coefficient, chosen (not fitted) by Barnes (2007), is a term that determines the color for wich the isochrone gives a period of 0 days. The new value of b is interesting as it corresponds to the approximate (B-V) color for late F-type stars, so at the transition from a radiative to a convective envelope ($M \sim 1.3 M_{\odot}$). In the case of the a and c coefficients the values found here are larger than those deirved by other authors and therefore the isochrone has slightly smaller curvature and larger slope.

It's useful to compare the Pleiades sample with data for other open cluster to test the general applicability of the relationship found. In Fig. 3.4, all clusters with ages $< 230 Myr$ considered are compared. Each cluster has a well defined I-sequence. For M34 and M35 Meibom et al. (2011) and Meibom et al. (2009) identified the stars on the I-sequence. The period-colour relationship found here and that of Barnes (2007) are shown for comparison.

Fig. 3.4 shows that the relation found matches very well the common mass dependence expecially from late-F to mid-K type. The main period-color sequences in the different clusters overlap. The reddest stars in the clusters exhibit a large dispersion in rotation rate.

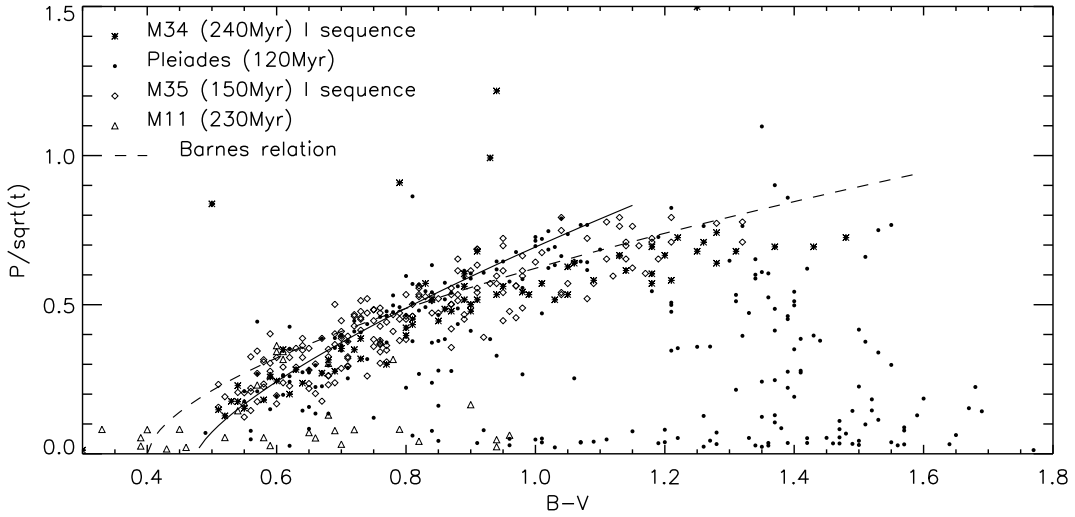

Figure 3.4: Plot of $P/\sqrt{t}$ vs. $(B-V)$ for open cluster stars with an age $120 \leq t \leq 230$Myr. Dashed line is the Barnes relationship, the solid line is the function derived in this work.

3.2 Uncertainties of the gyrochronology around the Pleiades' age

Following Barnes (2007), the rotation rate is given by $P(B-V,t) = f(B-V)g(t)$ where $f(B-V)$ and $g(t)$ are the color and age dependencies described in the Eq. (3.1). Taking logarithms and differentiating we have

$$\ln P = \ln f + \ln g \Longrightarrow \frac{dP}{P} = \frac{df}{f} + \frac{dg}{g} \tag{3.3}$$

It's possible to explicit the $f(B-V)$ and $g(t)$ functions.
Now, $f(B-V) = ax^c$ where $x = B-V-b$ and a,b and c are the fitted constants (with associated errors) listed in Table 3.1. Thus $df/f = da/a + cdx/x + dc\ln x$.
Now, $g(t) = t^n$ where $n = 0.5$. Thus $dg/g = ndt/t + \ln t dn$. Since there is no uncertainty associated with n, $dg/g = ndt/t$.

Substituting, rearranging and adding the errors under the usual assumption of independece yields

$$\left(n\frac{\delta t}{t}\right)^2 = \left(\frac{\delta P}{P}\right)^2 + \left(\frac{\delta a}{a}\right)^2 + \left(c\frac{\delta x}{x}\right)^2 + (\delta c \ln x)^2 \tag{3.4}$$

The period determination itself is not usually a great contributor to the error. Considering the Hartman et al. (2010) data for the Pleiades in the I-sequence the error for periods less than 12 d has a mean value of 0.02%, so in the worst case $\delta P = 0.0024$. For $\delta x = \delta(B-V)$ I adopt the value of 0.01 for the color, suggested by the percision

of the data. Inputting all these values in the Eq. (3.4)

$$\left(0.5\frac{\delta t}{t}\right)^2 = \left(\frac{0.0024}{P}\right)^2 + \left(\frac{0.020}{1.111}\right)^2 + \left(0.729\frac{0.01}{x}\right)^2 + (0.053\ln x)^2 \tag{3.5}$$

Thus,

$$\left(0.5\frac{\delta t}{t}\right)^2 = 10^{-4} \times \left[\frac{5.7\cdot 10^{-2}}{P^2} + 3.24 + \frac{0.531}{x^2} + 28.1\ln^2 x\right] \tag{3.6}$$

$$\frac{\delta t}{t} = 2\% \times \sqrt{\frac{5.7\cdot 10^{-2}}{P^2} + 3.24 + \frac{0.531}{x^2} + 28.1\ln^2 x} \tag{3.7}$$

Recalling that t is in Myr, P is in days, and $x = (B-V) - 0.476$ for 200 Myr old stars with different masses it's possible found (where it has been used the Barnes et al. (2010) mass-color relationship)

$$\frac{\delta t}{t} = \begin{cases} 5\%, & 0.65M_\odot \text{ (B-V)=1.27, P=10.7 d} \\ 10\%, & 0.8M_\odot \text{ (B-V)=0.98, P=7.8 d} \\ 20\%, & 1M_\odot \text{ (B-V)=0.66, P=4.3 d} \\ 30\%, & 1.1M_\odot \text{ (B-V)=0.57, P=2.8 days} \end{cases} \tag{3.8}$$

The behaviors of the errors, calculated using the Eq. (3.7), are such that the color and period errors dominate for bluer stars. The possibility of calculating the errors distinguishes gyrochronology from other method in calculating the age.

3.3 From 250 to 550 Myr

Having found that the relation (3.1) is valid for clusters younger than 250 Myr, let's see how it compares the older cluster. Overplotting the relation found and all the data available for the clusters with an age in the range $550Myr \leq t \leq 1Gyr$ one notes the breakdown of Skumanich law (see Fig. 3.5) and that the relation predicts rotation periods at least 50% longer than those observed in the clusters.

Despite the disagreement with the color-periods-age relation found for the Pleiades, all clusters still display distinct I and C sequences. The rich populations of early and mid-K dwarfs that were on the C-sequence have evolved onto the I-sequence, leaving the C-sequence and gap populated by late-K dwarfs. This change confirms Barnes' suggestion that K dwarfs have evolved onto the I-sequence during this age-gap between 250 and 550 Myr. However the older cluster do not slow down as expected. A possible explanation could be related to the internal angular momentum transport processes between the radiative core and the convective envelope, whose effect is to speed up the star.

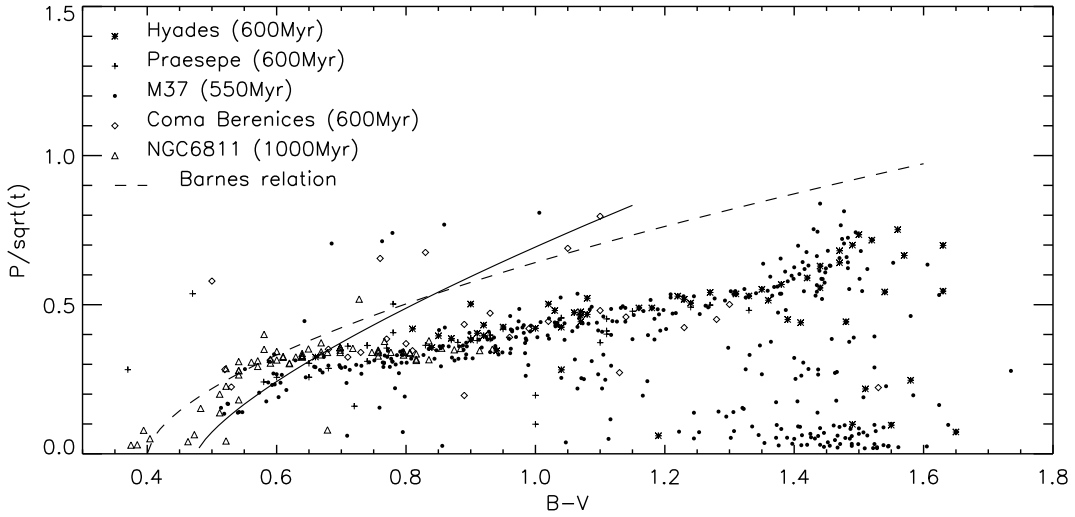

Figure 3.5: Plot of $P/\sqrt{t}$ vs. $(B-V)$ for open cluster stars with an age $550 \leq t \leq 600$Myr. Dashed line is the Barnes relationship, the solid line is the function derived in this work.

Accepting this as valid explanation and assuming that this process cannot be constant for all masses, an exponential age-dependence in addition to the Skumanich one has been tentatively introduced. The proposed relationship has the functional form:

$$P/\sqrt{t} = (t/t_0)^{n'(B-V)} \times a[(B-V)-b]^c \tag{3.9}$$

where a, b and c are the coefficients found in the previous section, t_0 is the Pleiades age (120 Myr) and n' is an exponential assumed to be (B-V) dependent. Among the older clusters, M37 is the most populated and luckily the I-sequence that starts from $(B-V) \sim 0.5$ and ends roughly at $(B-V) \sim 1.4$ is rather well-defined (Fig. 3.6).

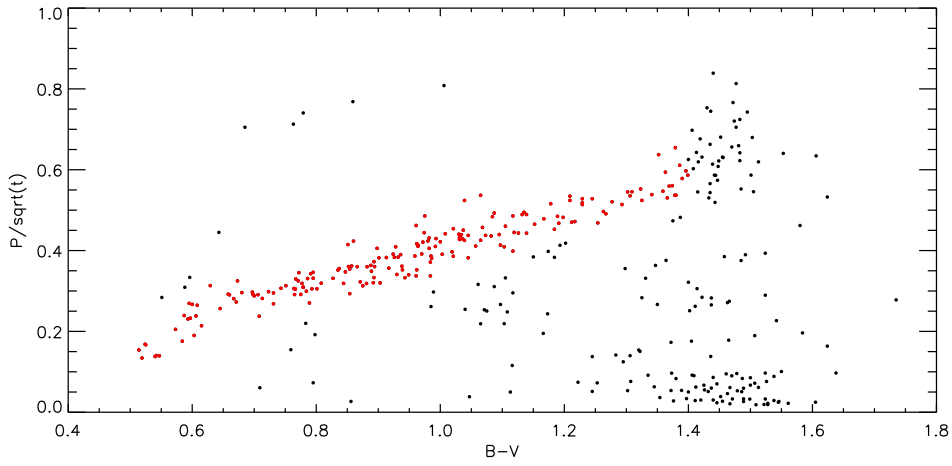

Figure 3.6: Rotation periods vs. (B-V) in the cluster M37. Periods are scaled to the square root of age (in Myr). With the red points the stars selected to be in the I-sequence and used for the fit.

The period-colour relation breaks down at the M-dwarf regime where stars become entirely convective (as already noted by Delorme et al. (2010)). At the blue end ($(B-V) \sim 0.5$) stars have rotation periods of $\sim 3.15d$ while at the red end ($(B-V) \sim 1.4$) stars have rotation periods of $\sim 15.35d$. Redward of $(B-V) \sim 1.4$ the maximum rotation period as a function of color continues to follow this sequence. However there is also a broad tail of stars with shorter and longer rotation periods. The fit, therefore, does not extend beyond $(B-V) = 1.4$, in the M-type regime where the different internal structure may cause a much larger dispersion in the rotational period. The exponential n' has been fitted using Eq. (3.9) (Fig. (3.7)). In Fig. (3.7) it's also plotted the n' value by considering the Sun ($(B-V)_\odot = 0.62$, $P_\odot = 27.7d$, $t = 4500Myr$ then $n' = 0.12$). First of all it's possible to say that a quadratic function, like $n' = u'(B-V)^2 + v'(B-V) + w'$, approximate in a rather satisfactory way the values found. The values found from the fit for this curve are listed in the Table 3.2 with respective errors.

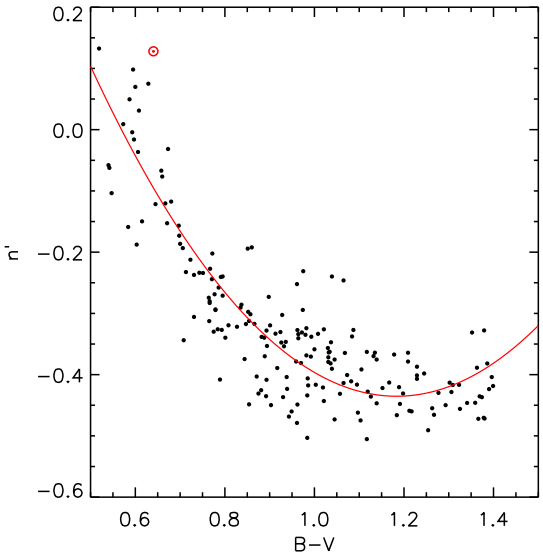

Figure 3.7: Values for the exponential n' found from eq. 3.9 vs. (B-V). With red line the quadratic fit for the values. With red $\odot$ symbol the value found for the Sun.

Table 3.2: Quadratic function coefficients and their errors derived from the fit made on n' parameter.

Coefficient	value	error
u'	1.180	0.076
v'	-2.729	0.162
w'	1.153	0.083

Note that n' in the range $0.5 \lesssim (B-V) \lesssim 0.7$ does not exceed the value of $|0.1|$. This means that up to $M \sim 1M_{\odot}$ type stars this kind of correction it's not necessary and the spin-down does not deviate much from the Skumanich law. Accepting the fact that a star loses memory of its initial rotation history once it reaches the MS, the value for n' implies that these stars rotate as solid body and lose angular momentum through a magnetized wind as described by Kawaler (1988). A different scenario applies to the K-type stars range. Here the value of this correction is greater. The negative value confirms the fact that the rotational period are shorter than predicted by only the Eq. (3.1). The values found for the coefficient, when $(B-V) \gtrsim 0.7$ in the M37 case, imply that $0.5 \lesssim (t_{M37}/t_0)^{n'} \lesssim 0.7$ otherwise the stars rotate from 1.4 to 2 times faster than predicted by Skumanich law.

Adding this new information it is possible to rewrite the relationship that relates, through the color index (B-V), the rotational periods to the age:

$$P/\sqrt{t} = (t/t_0)^{0.223(B-V)^2-0.536(B-V)+0.226} \times 1.111[(B-V)-0.476]^{0.729} \qquad (3.10)$$

The plot of this function is shown in Fig. 3.8. The dotted line is to highlight that for $(B-V) \geq 1.4$ the relationship is extrapolated. In Fig. 3.9 this relation is overplotted with all the clusters data considered for this work.

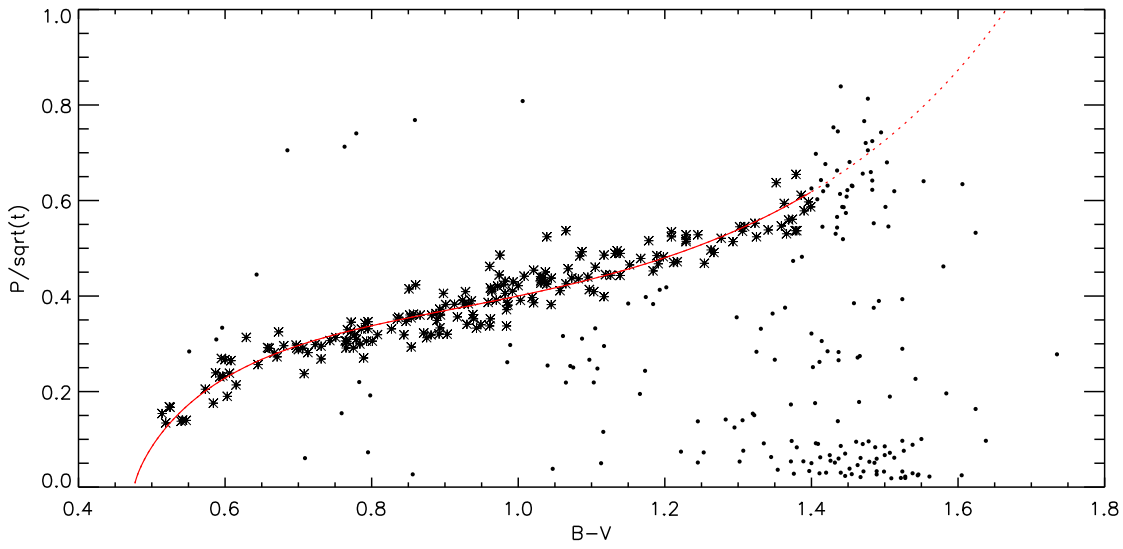

Figure 3.8: Rotation periods vs. (B-V) in M37 cluster. Periods are scaled to the square root of age. With asterisks the stars selected to be in the I-sequence. The relationship defined by eq. 3.10 is shown as solid line. The relation is extrapolated for $(B-V) > 1.4$ and shown as dotted line.

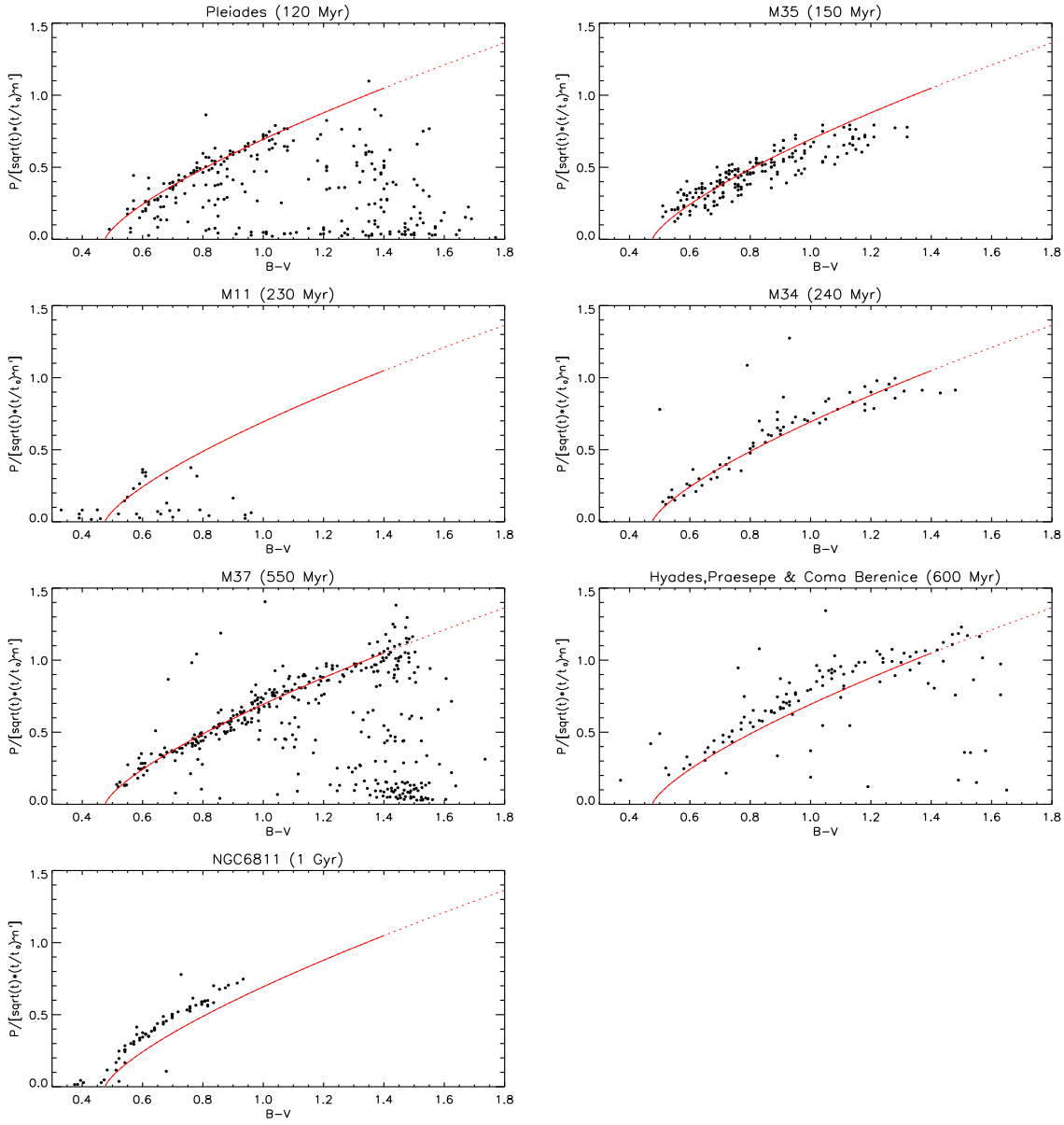

Figure 3.9: Rotation periods vs. (B-V) in all clusters considered. Periods are scaled to the part of the relation age-dependent $g(t, B-V) = \sqrt{t}\left(\frac{t}{t_0}\right)^{n'(B-V)}$.

3.4 From 550 Myr to 1 Gyr

The relationship (3.10) works well from the Pleiades to the M37 age, while are underestimate the values of rotational periods for older cluster. This behavior suggests that 550 Myr could be the core-envelope angular momentum coupling time-scale. Then, assuming that stars continue to lose angular momentum through Kawaler (1988) law throughout their life and that the process that speeds up them from 550 Myr stops, the relationship for the periods could be written in the following way:

$$P/\sqrt{t} = (t_{M37}/t_0)^{n'(B-V)} \times a[(B-V) - b]^c \tag{3.11}$$

The result is shown in Fig. 3.10

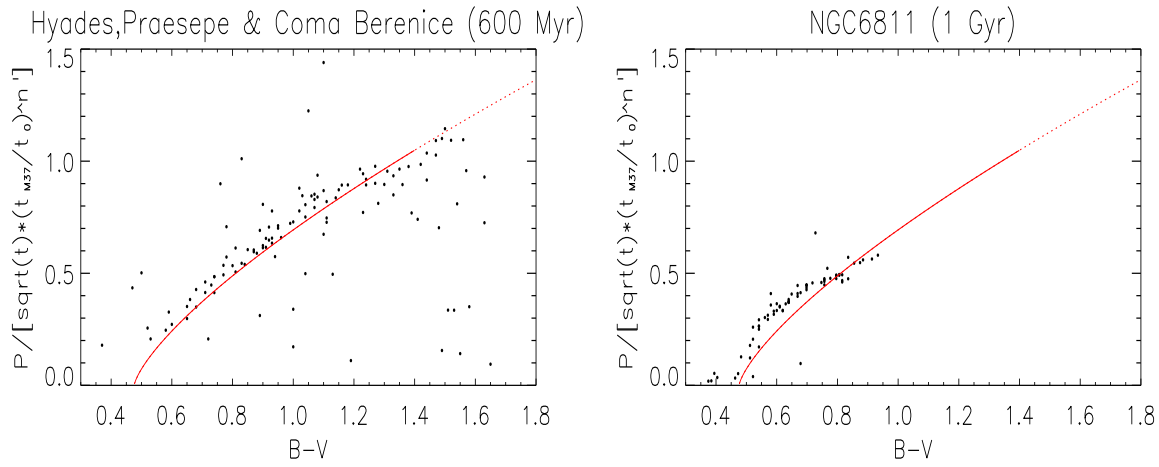

Figure 3.10: Rotation periods vs. (B-V) in clusters older than M37 (550 Myr). Periods are scaled to the part of eq. 3.11 age-dependent *g(t)* ($g(t) = \sqrt{t} \times (t_{M37}/t_0)^{n'(B-V)}$).

Despite the loss of angular momentum, Eq. (3.11) still predicts rotation periods shorter than those observed in clusters with age $\simeq 600 Myr$. To describe this empirically another exponential age-dependence has been added to Eq. (3.11). The periods relationship has now the functional form:

$$P/\sqrt{t} = (t_{M37}/t_0)^{n'(B-V)} \times (t/t_{M37})^{n''} \times a[(B-V)-b]^c \qquad (3.12)$$

Since NGC6811 is the oldest cluster available it has been used to determine n''. The fit does not obviously extend beyond $(B-V) = 0.95$. Using periods of star with $(B-V) > 0.476$, the exponential n'' has been fitted (Fig. (3.11)) together with n'' obtained from the M37 and the Sun period ratio ($(B-V)_\odot = 0.62$, $P_\odot = 27.7d$, $t = 4500 Myr$ then $n'' = 0.25$). As for n' a quadratic function has been used to approximate, $n'' = u''(B-V)^2 + v''(B-V) + w''$. The coefficients found from the fit for this curve are listed in Table 3.3 with the respective uncertainties.

Table 3.3: Quadratic function coefficients and their errors derived from the fit made on n'' parameter.

Coefficient	value	error
u''	3.927	0.909
v''	-7.786	2.637
w''	3.748	1.874

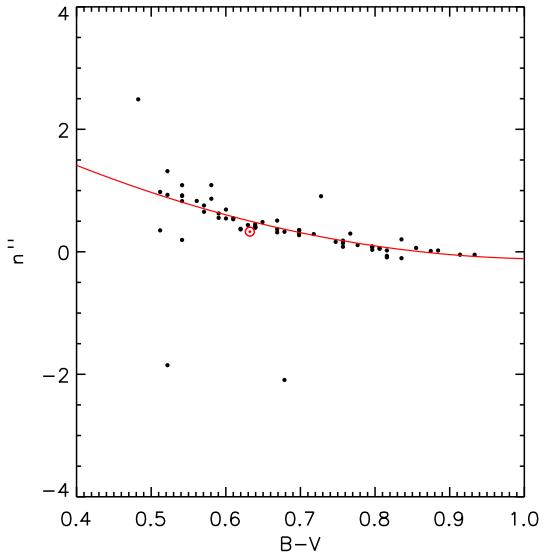

Figure 3.11: Values for the exponential n'' found from eq. 3.12 vs. (B-V). With red line the quadratic fit for the values.

The entire range n'' it's roughly between 0 and 1. The comparison of Eq. (3.12) with the data at 600Myr and 1 Gyr is shown in Fig. 3.12. The dotted line highlights the extrapolation for $(B-V) \geq 0.95$. The diverging trend of the function, for redder stars, is due to lack of data that would have constrained the n'' fit. Summarising all the relationships that correlate, through the color index (B-V), the rotational periods to the age (until 1 Gyr):

$$P = \begin{cases} \sqrt{t} \times (t/t_0)^{n'(B-V)} \times a[(B-V)-b]^c & (a) \\ \sqrt{t} \times (t_{M37}/t_0)^{n'(B-V)} \times (t/t_{M37})^{n''(B-V)} \times a[(B-V)-b]^c & (b) \end{cases} \quad (3.13)$$

Where Eq. (a) is used when $120Myr \leq t \leq 550Myr$ and Eq.(b) when $550Myr \leq t \leq 1Gyr$, Fig. 3.13 compares rotational periods evolution, for $0.6M_\odot$, $0.8M_\odot$ and $1M_\odot$, under the relationship expressed in eq. 3.13. For a solar mass star it's also shown the Skumanich relationship.

3.5 Discussion

The stellar rotation is a promisinig tool for estimating the age of Sun-like stars. The upper mass limit for rotation-age relations is set by the F star transition from deep to shallow surface convective zones. It's not clear if stars more massive than $M \sim 1.2M_\odot$ have a rotation-age relationship, and it's difficult to detect rotation periods signal for stars more massive than the Sun because the fractional star spot coverage, and the amplitude of variability, drop steeply for hotter stars. The relations work for stars below the F type and above the fully convective limit, the

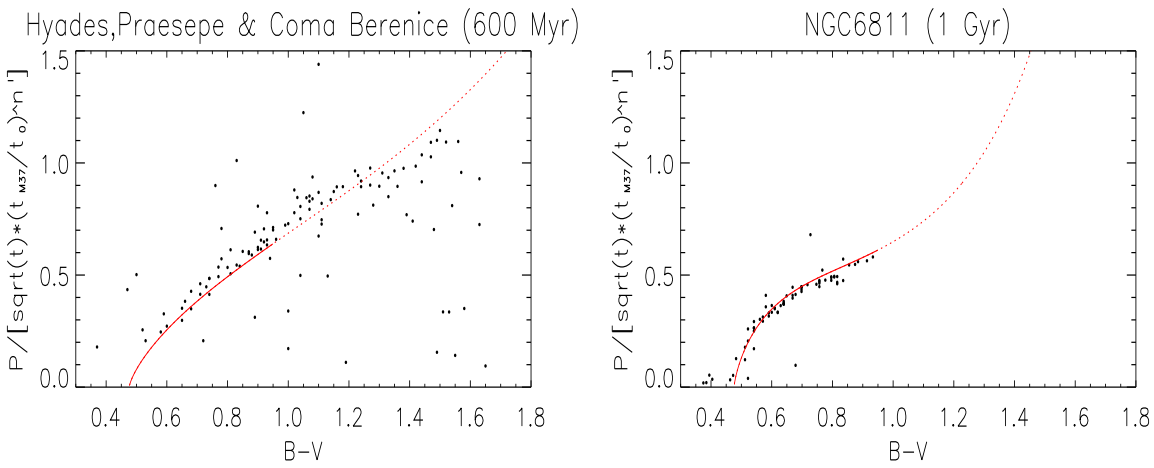

Figure 3.12: Rotation periods vs. (B-V) in NGC6811 cluster. Periods are scaled to the part of eq. 3.11. age-dependent *g(t)* ($g(t) = \sqrt{t} \times (t_{M37}/t_0)^{n'(B-V)}$). The relationship defined by eq. 3.12, with the fitted values for the n'' coefficient, is shown as solid line. The relation is extrapolated for $(B-V) > 0.95$ and shown as dotted line.

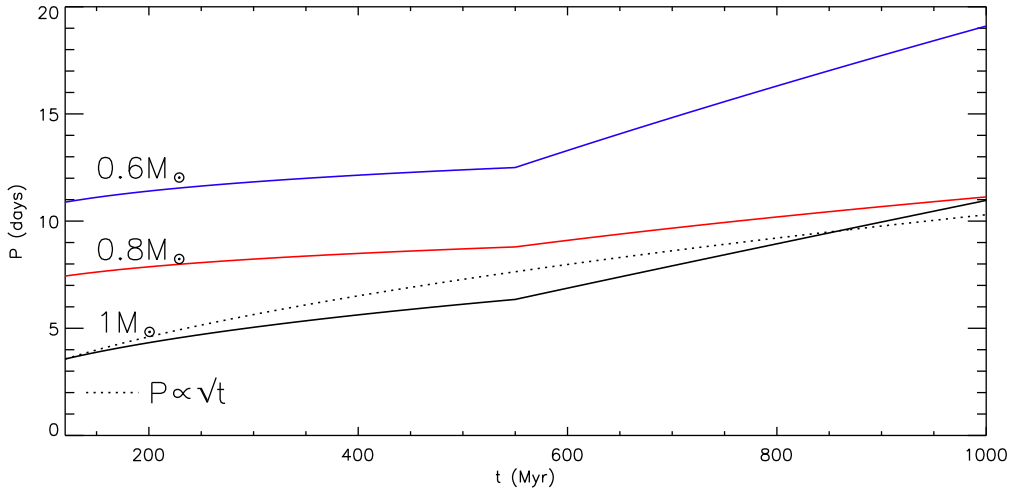

Figure 3.13: Rotation periods evolution according to eq. 3.13 (solid lines) for a $0.6M_{\odot}$, $0.8M_{\odot}$ and $1M_{\odot}$ star. The dotted line gives the $1M_{\odot}$ calibrated Skumanich $P \sim \sqrt{t}$ relation.

M-dwarfs regime that puts strong constraints on theoretical models. These age-rotation period relations cannot be applied to derive measurement of the age of stars younger than their magnetic breaking convergence time (this physical condition sets the stars that belong to I sequence). As found by Delorme et al. (2010) these limits are $\sim 150Myr$ for F and G dwarfs and $\sim 600Myr$ for late-K and early M dwarfs.

These relationships are calibrated to clusters in a limited age-range, but could be used easily in simulation about angular momentum evolution until 1Gyr. Unlike observational data, the temporal coverage is continuous and for $120Myr \leq t \leq 1Gyr$ is

able to reproduce the real spread in the rotational periods through the uncertainty found with propagation of errors. Assuming the errors for n' and n'' as constants and equal to the average dispersion around the fit, $\delta n' = 0.15$ and $\delta n'' = 0.27$, and remembering that $x = (B-V) - b$, $\delta x = 0.01$, it's possible write

$$\delta P = \begin{cases} P \times \sqrt{\left[\delta n' \ln \frac{t}{t_0}\right]^2 + \left[\frac{\delta a}{a}\right]^2 + \left[c\frac{\delta x}{x}\right]^2 + [\delta c \ln x]^2} & (a) \\ P \times \sqrt{\left[\delta n' \ln \frac{t_1}{t_0}\right]^2 + \left[\delta n'' \ln \frac{t}{t_1}\right]^2 + \left[\frac{\delta a}{a}\right]^2 + \left[c\frac{\delta x}{x}\right]^2 + [\delta c \ln x]^2} & (b) \end{cases} \tag{3.14}$$

Where eq. (a) is used when $120Myr \leq t \leq 550Myr$ and eq. (b) when $550Myr < t \leq 1Gyr$.

Unfortunately this relationship is not sun-calibrated and the rotational period obtained for the Sun is not correct at all. We know that (Cox (2000)): $(B-V)_\odot = 0.62$, $t_\odot \sim 4500Myr$ and $P_\odot \sim 27.7d$ (it's a mean value between poles and equator rotational periods). Calculating the rotational period that could have a star like the sun using eq. 3.13 one can found $\sim 50d$. It's extremely large, about twice that observed. Also considering only angular momentum loss trough Kawaler (1988) law, eq. 3.11, the result is not encouraging. This time $P \sim 16d$, about half of that observed.

This fact highlights how it's difficult to constrain the behavior of rotational periods throughout the whole stars' life. The loss of angular momentum through the Kawaler (1988) law is not enough. In this work has been necessary to introduce a factor that, till M37's age, quicken stars and another, having an effect from 550 Myr to NGC6811's age, that that slow down stars. A number of new models on origin and evolution of stellar angular momentum have been proposed in recent years. I reserve for the future the aim to work on a rotational clock that takes into account the new formulation for angular momentum evolution proposed by Reiners et al. (2012) and Gallet et al. (2013).

Contrary to Kawaler (1988), that assumes that angular momentum loss is entirely independent of the radius, Reiners et al. (2012) account rotation related to magnetic field strength instead of to magnetic flux, this includes a strong dependence on the stellar radius R as being vital to understand magnetic braking. Gallet et al. (2013) presented a model that, unlike previous, estimates angular momentum loss on the recent stellar wind simulation performed by Matt et al. (2012) and assumes the stel-

lar magnetic field, generated by dynamo process, following Cranmer et al. (2011) prescriptions also for the mass-loss rate. Kawaler (1988) wind law were based upon analytic or semi-analytic calculations that necessarily relied upon several simplifyng assumptions, such as that of spherical symmetry and a priori specification of the magnetic geometry. Matt et al. (2012) used multi-dimensional, magnetohydrodynamical (MHD) simulations for computing wind solutions.

Chapter 4

Rotational dependence of Lithium depletion

It is known that the surface lithium abundances of field solar-analog dwarfs show a large dispersion despite the similarity of stellar parameters. The aim of this part of work is to exploit the relationships found in Chap. 3 for relating the lithium depletion to the rotational history of a star. From previous work we know that hydrodynamical instabilities acting on various timescales are responsible for the so-called rotationally-driven mixing that increases the efficiency of lithium burning in stellar interiors. In this respect a key result is the observed relationship between Li abundances and rotation in young stars. Soderblom et al. (1993b) report that fast solar-type stars in the Pleiades exhibit higher Li abundances than slow rotators. Taken at face value, this result indicates that Li depletion already takes place during the PMS, and is more pronounced in slow rotators than in fast ones. Hence, rotationally-induced mixing appears more efficient in slow rotators. This result suggests that rotational mixing is primarily driven by the rotational shear at the base of the convective envelope: slow rotators are observed to be more Li-depleted on the ZAMS than fast rotators and the models presented by Bouvier (2008) indicate that they experience stronger core-envelope decoupling. In contrast, fast rotators lose more angular momentum at the stellar surface and also transfer angular momentum more efficiently from the core to the envelope. da Silva et al. (2009) studing the Li depletion in the pre-main sequence, using nine associations with ages between $\sim 6 Myr$ and 70 Myr, found that for stars with $v \sin i$ above $20 kms^{-1}$ rotation seems to play an important role in inhibiting the Li depletion.

To investigate the behaviour of these phenomena, it was made an extensive study of Li abundances and their dependence on the stellar parameter rotation period for the

homogeneous sample of 102 Pleiades's stars selected by Sestito et al. (2005). Both rotation and lithium depletion have mass dependence and time dependence. The idea at the basis of this work's part is to investigate what is the amount of rotation contribution on lithium depletion once it's removed the age and mass contribution from the data trend.

4.1 Lithium abundance data and models

Since in this work's part will be used data took from different authors, to go to any length to make the analysis coherent, it has been decided to use the Hartman et al. (2010) (B-V) photometry since it's more recent than that of Sestito et al. (2005) (that are taken from the original paper made by Soderblom et al. (1993b)). It has been rejected from the analysis the stars for which the difference between the two color value is more than $0.07mag$. The comparison between the different (B-V) color index (figure 4.1) shows that the Hartman et al. (2010) values are on average $0.037mag$ greater than the Sestito et al. (2005) ones.

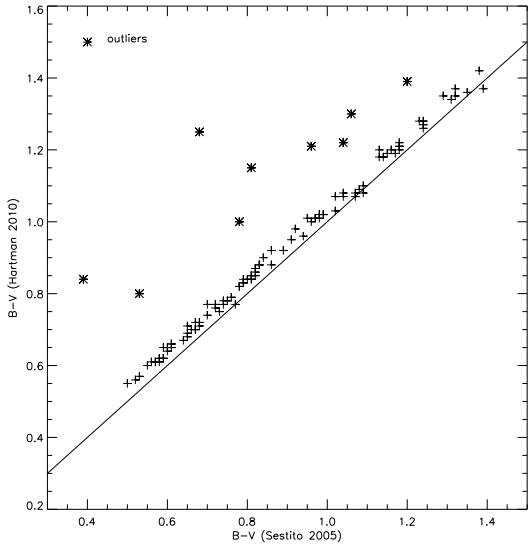

Figure 4.1: Comparison of Hartman et al. (2010)(B-V) color index to those reported in Sestito et al. (2005) (taken from the original paper made by Soderblom et al. (1993b)). The asterics are the stars rejected from the analysis because the difference between the two values for the color index is greater than 0.07mag.

This difference in the (B-V) color leads the temperature and the abundance derived from Hartman et al. (2010) to be respectively smaller of about $\sim 100K$ and $\sim 0.2dex$. Since this difference is not relevant for the analysis presented in the following, the abundances have not been recalculated and the Sestito et al. (2005) values are adopted throughout.

Lithium depletion is not a continuous process that can be described with a $t^{-\alpha}$ law, for this reason several non-standard processes have been proposed in recent years to be included in models: outer boundary conditions based on non-grey atmosphere models (e.g. Baraffe et al. (1998)); miscroscopic diffusion, determining the separation of atomic species in the stellar gas (e.g., Chaboyer et al. (1995)); mass loss trough stellar winds; effects associated with the pressure ionization and the degeneracy in stellar interior (e.g., Siess et al. (2000)); gravity waves to determine the micro-turbolence velocity (e.g., Allard et al. (2011)). As for the PMS phases the amount of Li destroyed in this stage is a strong function of the assumed input physics in the models; different models result into distinct amount of PMS depletion and thus into disparate A(Li) values on the ZAMS.

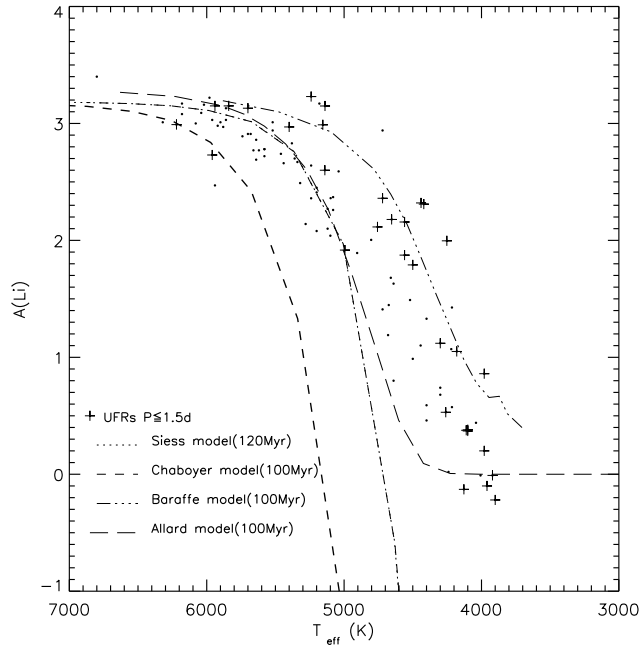

Figure 4.2: Lithium abundances vs. T_{eff} for the Pleiades cluster. The cross symbols are ultra-fast rotators ($P \leq 1.5$days). Dotted line is the Siess et al. (2000) model for 120 Myr. Dashed lines Chaboyer et al. (1995) model for 100 Myr without and with overshooting. Dot-dashed line is the Baraffe et al. (1998) model for 100 Myr. Long dashed line is the Allard et al. (2011) model for 100 Myr.

From figure 4.2, that shows the models and the sample, it's possible notice that Baraffe et al. (1998) and Allard et al. (2011) models reproduce respectively the upper and lower bounds for the distribution of data. Analyzing the data distribution it's possible to say that for $T_{eff} \gtrsim 6000K$ ($M \gtrsim 1.3M_{\odot}$) the stars have essentially the same Li abundance ($A(Li) \approx 3.2 - 3.3$) so that they don't experience any pre-main sequence Li depletion. Stars above $\sim 1.1M_{\odot}$ have a little PMS depletion. A great

spread exists primarly for $M \lesssim 0.9 M_{\odot}$ and it grows with decreasing mass. In this mass range the slow-rotating stars have a considerably great dispersion. There are

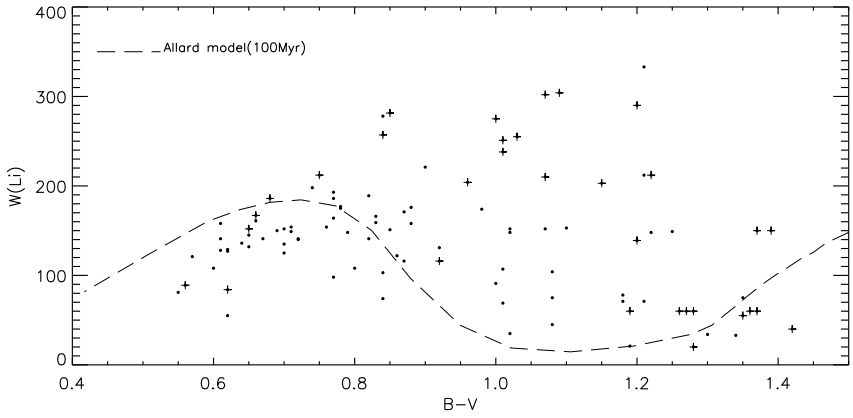

Figure 4.3: Observed equivalent widths of the Li I λ6708 ($m\mathring{A}$) vs. (B-V) color for stars of the Pleiades. The cross symbols are ultra-fast rotators ($P \leq 1.5$days). The dashed line represents the Allard model for 100 Myr.

no stars that have Li abundances that exceed the "primordial" value in a significant way. For the Pleiades late-F and G dwarfs, $0.50 \lesssim (B-V) \lesssim 0.75$, the scatter in W_{λ}(Li) is modest. At $(B-V) \approx 0.8$ the situation changes dramatically, with a sudden increase in the spread in W_{λ}(Li). This scatter grows with color reaching the maximum for $(B-V) \gtrsim 1.0$. Both figure 4.2 and figure 4.3 show that there is a strong tendency for the ultrafast rotators to be Li rich, confirming the correlation between excess Li and excess rotation put by Butler et al. (1987). The fact that fast rotators are well descripted by models is a direct result of what observed by Denissenkov et al. (2010). Rotation period distributions of low-mass stars in open clusters do not seem to support the hypothesis that all solar-type stars evolve as solid body rotators. Only the fastest rotators among solar-type stars can be considered to possess solid body rotation during their entire evolution, whereas their slowly rotating counterparts are most likely to manifest internal differential rotation between the ages of ~ 30 Myr and several hundred Myr. As also noted by Bouvier (2008) the consequence of this different core-envelope coupling is that slower rotators should exhibit more significant Li depletion than rapid rotators.

4.2 Analysis of the Lithium-rotation correlation

For the analysis, to reduce the effects maybe due to different stars' spectral type and so to different structure, the entire (B-V) range has been divided in 5 bins:

1. G type stars with $0.58 \leq (B-V) < 0.74$;
2. early K type stars with $0.74 \leq (B-V) < 0.91$;
3. mid- and late-K type stars with $0.91 \leq (B-V) < 1.15$;
4. early M type stars with $1.15 \leq (B-V) < 1.25$;
5. mid-M type stars with $1.25 \leq (B-V) < 1.45$.

To remove the mass dependence from the rotational periods the residuals of periods from Eq. (3.2) have been considered. Fig. 4.4 shows the Li abundance and W(Li) vs. such period residuals. The correlation is here quantified using the Pearson coefficient, which is a measure of the linear correlation between two variables X and Y. The coefficient varies between +1 and -1 inclusive, where 1 is total positive correlation, 0 is no correlation, and -1 is negative correlation. This is widely used as a measure of the degree of linear dependence between two variables.

In Fig. 4.4 the correlation's slope is negative for all mass bins showing that the faster rotators in each bin are always those who have more lithium. The values found for the Pearson coefficient display that the correlation is not present in stars with $1.25 \leq (B-V) \leq 1.45$. Pearson coefficient values more or less significant are found for all other mass bins. The values found for this coeffcient are systematically a little larger when it is considered the W(Li), instead of abundance. This is explained throughout a smaller dispersion around the regression line for W(Li) measurements. Fig. 4.2 shows that the lithium abundance has a rude decrease when temperature changes from 5000 to 4000 K. Having considered 5 mass bins may not have been sufficient to remove the mass dependence from lithium abundance trend. For this reason, as done for rotational periods, the residuals of lithium abundances from Baraffe et al. (1998) and Allard et al. (2011) models have been considered. Have been chosen these models because are the two that reproduce in the best way possible the trend of the data.

The result of this procedure is shown in figure 4.5. The two models return roughly the same values for Pearson coefficient also if they approach the data in different way. The biggest difference is found in the range $0.74 \leq (B-V) < 0.91$ where adopting the Allard model it's possible obtain a quite strong correlation (Pearson coefficient = -0.69). Having found again Pearson coefficient values that reveal the presence of correlation is a proof that the correlation found is real and not an effect

mass dependent.

Another possible internal error in the analysis could be that one done by the estimates of T_{eff} from the (B-V) colors. This uncertainty could be translated to a Li abundance error by rederiving it with T_{eff}. Make use of fundamental stellar properties such as equivalent width and color magnitude prevent the results from being affected from internal errors. For this purpose the residuals of W(Li) from Allard et al. (2011) model (Fig. 4.3) have been considered. Unfortunately, this is possible using the Allard et al. (2011) model only, since the Baraffe et al. (1998) relationship vs. (B-V) is not available to us. Fig. 4.6 shows the final correlations. What is observed is that the Pearson coefficients values have, once again, the same values. At this point can be stated that all the factors that could invalidate the results were taken into account. The presence of a real correlation can therefore be confirmed.

4.3 Discussion

The empirical rotation-mass relationship found for the Pleiades in Chap. 3 (Eq. (3.2)) allowed to remove the mass-dependence of rotation in the Li-rotation correlation analysis. Theoretical models of the Li-depletion allowed to remove the Li-abundance mass dependence too. Such an approach allowed to describe the Li-rotation correlation in more details than before.

The correlation appears to be a rather continuous one, as opposed to a systematic difference between the ultra-fast rotators A(Li) and that in all other stars. However, the correlation is almost non existent in the two ranges $0.58 \leq (B-V) < 0.74$ and $1.25 \leq (B-V) < 1.45$ where there is not a big spread in lithium equivalent widths values from that predicted by the models. For stars in these mass bins be slow or fast rotators don't affect their lithium depletion. Begins to be a soft correlation when it's considered the range between K and M type stars. The correlation is statistically significant in the $0.74 \leq (B-V) < 1.15$ color range. This range pratically corresponds to the range where the Pleiades I-sequence and main sequence are well populated.

The results are robust with respect to the models and assumptions adopted. In fact the same level of correlation is found without assuming a mass dependence of A(Li) from models or assuming such mass-dependence adopting different models for

the Li-depletion at the age of the Pleiades. The test carried out using W(Li) rather than A(Li), which has a shallower dependence on mass, reinforce such conclusions.

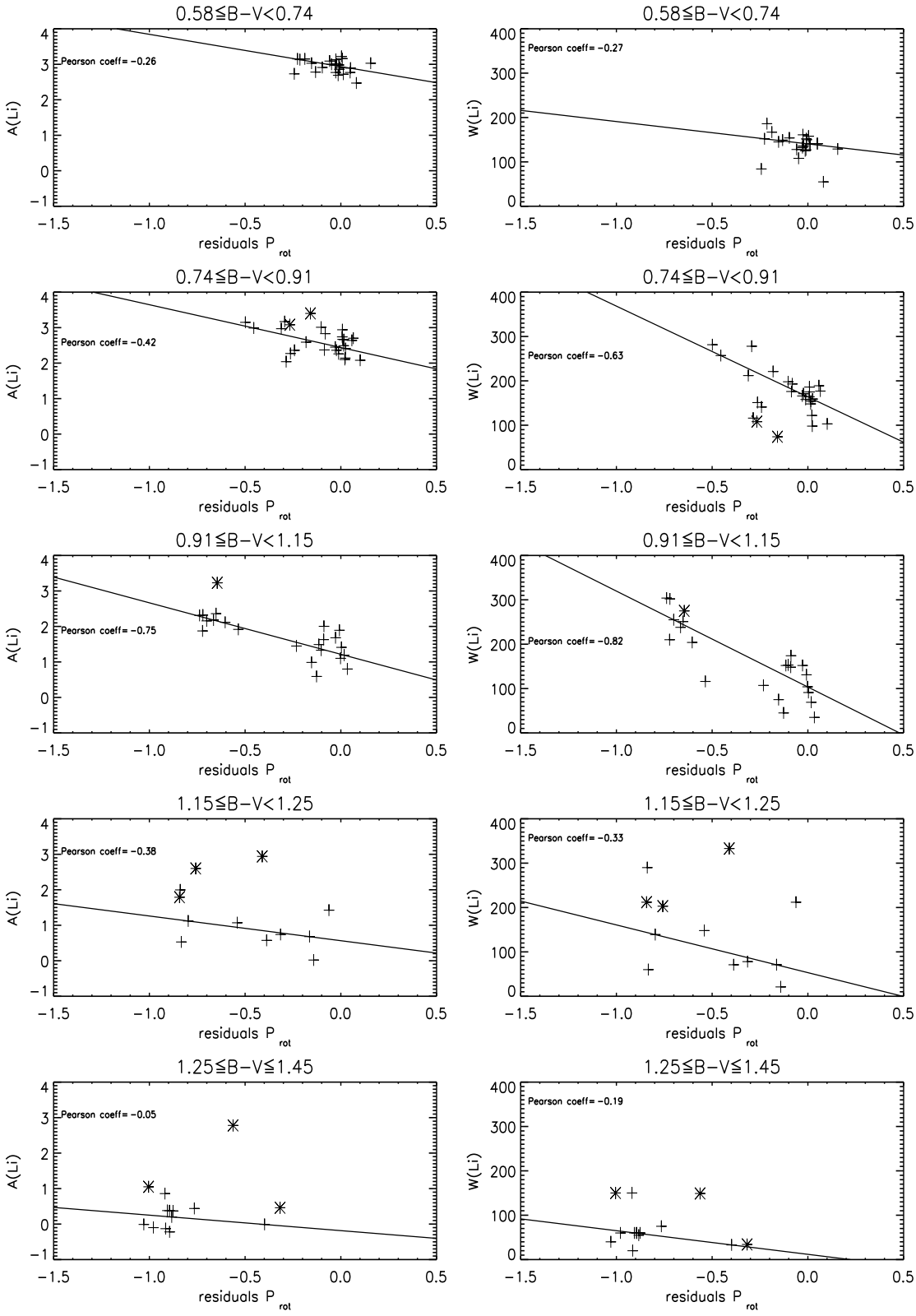

Figure 4.4: Lithium abundances and lithium equivalent widths as functions of differential rotational periods ($P-P_{fit}$) for different (B-V) color bins. The asterics are the stars rejected from the analysis because the difference between the two values for the color index is greater than 0.07mag.

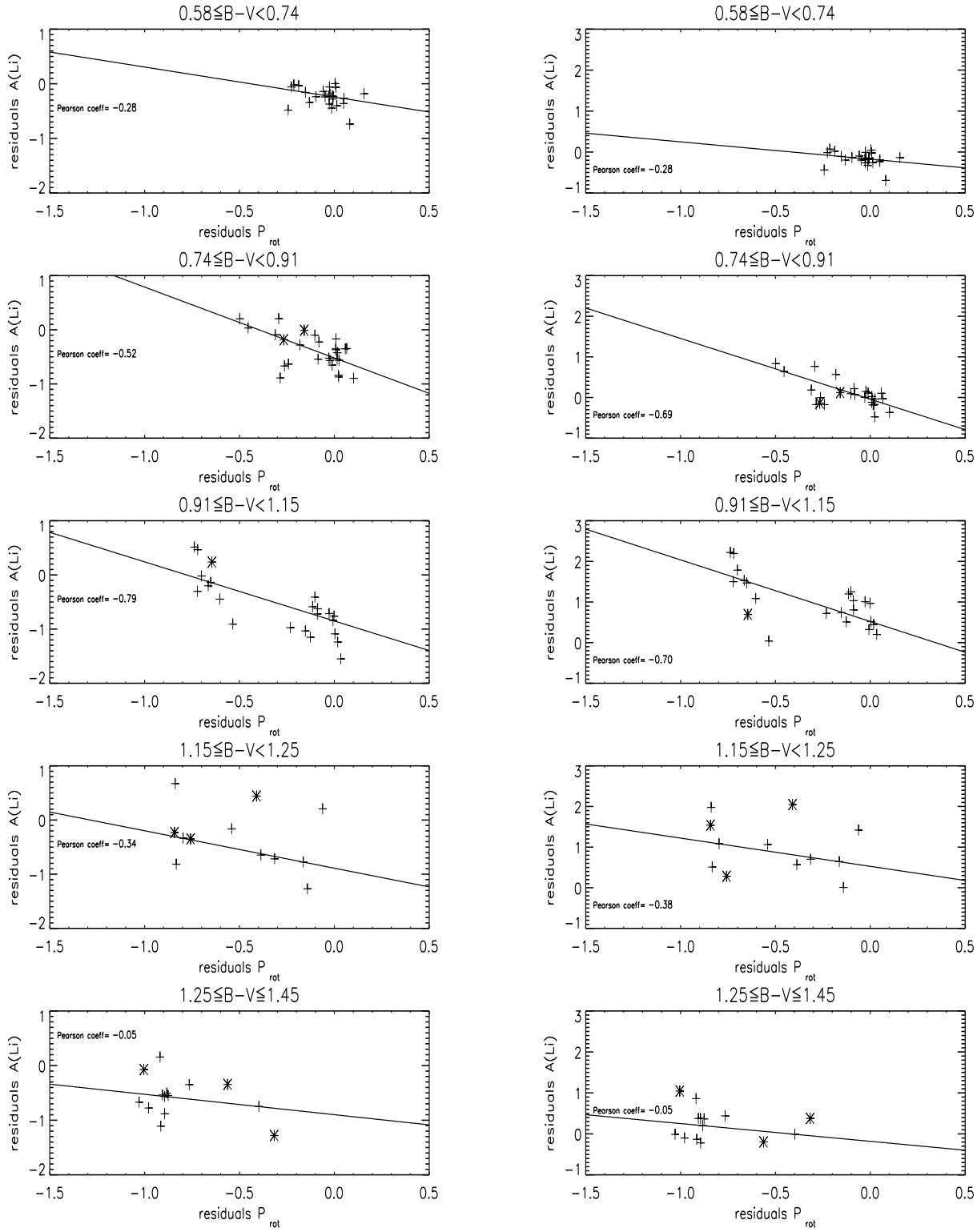

(a) Baraffe model (b) Allard model

Figure 4.5: Differential lithium abundance (from Baraffe (a) and Allard (b) models) as functions of differential rotational periods ($P - P_{fit}$) for different (B-V) color bins. The asterics are the stars rejected from the analysis because the difference between the two values for the color index is greater than 0.07mag.

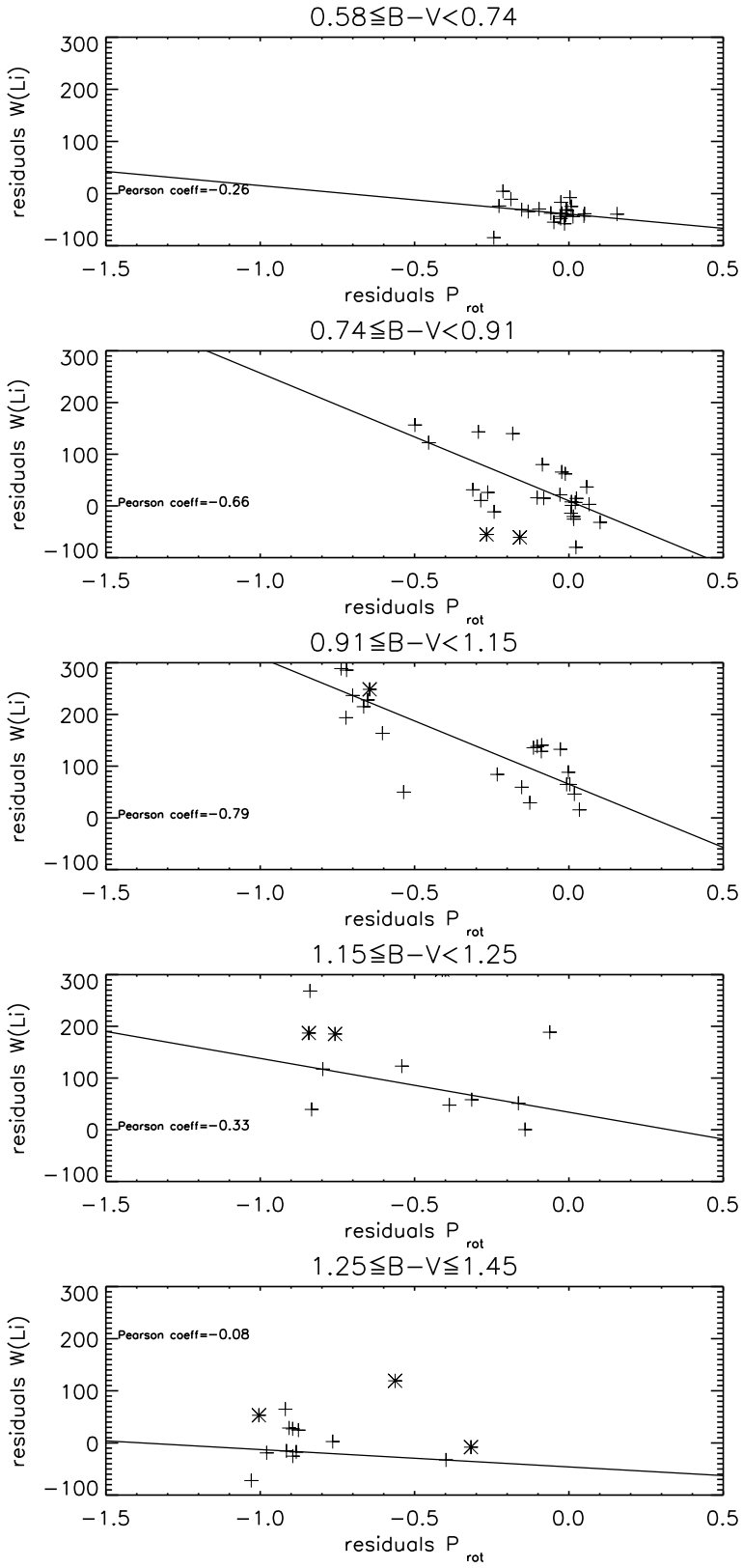

Figure 4.6: Differential lithium equivalent widths (from Allard model) as functions of differential rotational periods ($P - P_{fit}$) for different (B-V) color bins. The asterics are the stars rejected from the analysis because the difference between the two values for the color index is greater than 0.07mag.

Chapter 5

The age of the young loose association AB Doradus

The Local Association is a supercluster (stellar aggregates characterized by parallel space motions of their members) located within a radius of a few hundred parsecs around the Sun and often referred to as the Pleiades supercluster because of the similarity of the space motions of its members and the Pleiades open cluster. With recent identifications of relatively small nearby groups or associations of post T-Tauri stars with ages from 8 to 50 Myr located within 100-150 pc of the Sun can be said that a new stage of investigation of the structure of the Local Association has begun. AB Doradus is the nearest identified moving group. The age is important for understanding several key questions, for example the origin of the group or in studies of the properties of planetary systems compared with those existing in other systems. For AB Doradus two raher different estimates for its age have been proposed: the first one, of order of 50 Myr, by Zuckerman et al. (2004) and the second one of about 100-125 Myr by Luhman et al. (2005).

Zuckerman et al. (2004) began a spectroscopic search for young stars near the Sun and found that the space motion of the AB Dor moving group is clearly distinguished from that of the other young groups. They estimated the age in two ways. First comparing the intensity of H_α emission (and absorption) of the late-K and early-M type stars in the Tucana association with those of the group. Second, plotting three M type members of the AB Dor group on an M_K vs. (V-K) diagram, underlined that if Tucana is $\sim 30Myr$ then AB Dor stars are older but younger than ZAMS for M stars so are probably $\sim 50Myr$ old. Torres et al. (2008) estimated independently the age, from M_V vs. (V-I) and W(Li) vs. (V-I) diagram, giving the approximated value of $\sim 70Myr$. Luhman et al. (2005) have argued that the Lithium equivalent

width and $v \sin i$ of AB Dor are similar to the values observed for rapidly rotating K dwarfs in the Pleiades. In addition, the H_α emission strengths for the M-type members are indistinguishable from measurements in the Pleiades. Thus, these age diagnostics are consistent with the coevality of the AB Dor group and the Pleiades. Since very young open cluster are often found to be surrounded by unbound OB associations (Garmany (1994)), Luhman et al. (2005) suggested that the system identified by Zuckerman et al. (2004) as members of a moving group with AB Dor are probably the remnants of unbound OB and T associations connected with the star-formation event that formed the bound Pleiades open cluster, and so are somewhat older (75-150 Myr).

This common origin of the AB Dor Association and the Pleiades has been recently reinforced by Ortega et al. (2007), using Galactic dynamics calculations. This common origin would have occurred 119±20 Myr ago at a height of about 250 pc below the Galactic plane. The size of the birth region of Pleiades and AB Dor yielded by their dynamical solution could be explained within the framework of the open cluster formation scenario where a bound and an unbound system are born together. They suggest that the unbound system expanding at formation could be identified with the AB Dor group. This overall picture is in agreement with the conclusion of Luhman et al. (2005). As their arguments are based on the Zuckerman et al. (2004) list of members it will be important to revisit the question of the origin of the AB Dor Association on the basis of the new and more accurate measurements presented here.

5.1 The AB Dor age from stellar rotation

Given that one of the main aim of this thesis work is the re-calibration of the rotational clock (eq. 3.13), to resolve this discrepancy on age for the AB Dor group, has been used the comparison of distribution periods with that of the Pleiades to search for an evidence that could be useful in AB Dor age determination. The same comparison has been already done by Messina et al. (2010) but their Pleiades data were not as numerous as those that are now available.

In the two panels of Fig. 5.1 are reported the rotational model, the Pleiades rotational periods and those of AB Dor scaled to the part of Eq. 3.13 age-dependent $g(t)$ ($g(t) = \sqrt{t} \times (t/t_0)^{n'}$ where t_0 is the Pleiades age 120 Myr). It has been plotted

the behaviour of AB Dor in the two different cases, when age is considered to be 70 and 120 Myr. Eq. 3.13 has been calibrated on clusters older than 120 Myr but it has been supposed that the relationship could be extrapolated till 70 Myr.

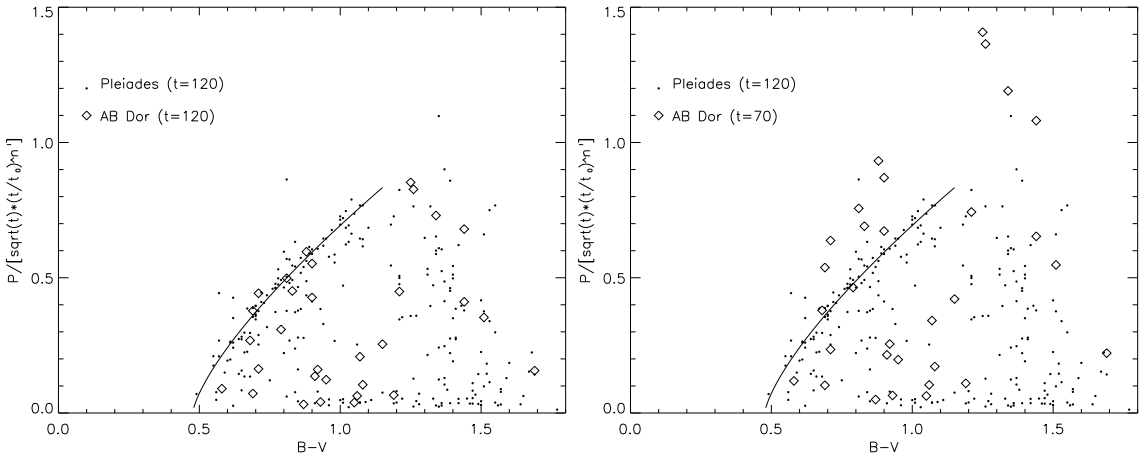

Figure 5.1: Comparison of the AB Dor rotaion periods vs. (B-V) relationship with the Pleiades. Rotation are scaled to the part of eq. 3.13 age-dependent *g(t)*. Rhombus symbols are AB Dor stars and dots are Pleiades members. In the left panel AB Dor is assumed to have the same age as the Pleiades (120 Myr). In the right panel AB Dor is assumed to have an age of 70 Myr.

If the assumption that Eq. 3.13 could be extrapolated till 70 Myr is wrong then $g(t) = \sqrt{t}$. Fig. 5.2 reports again the behaviour of AB Dor when age is considered to be 70 and 120 Myr.

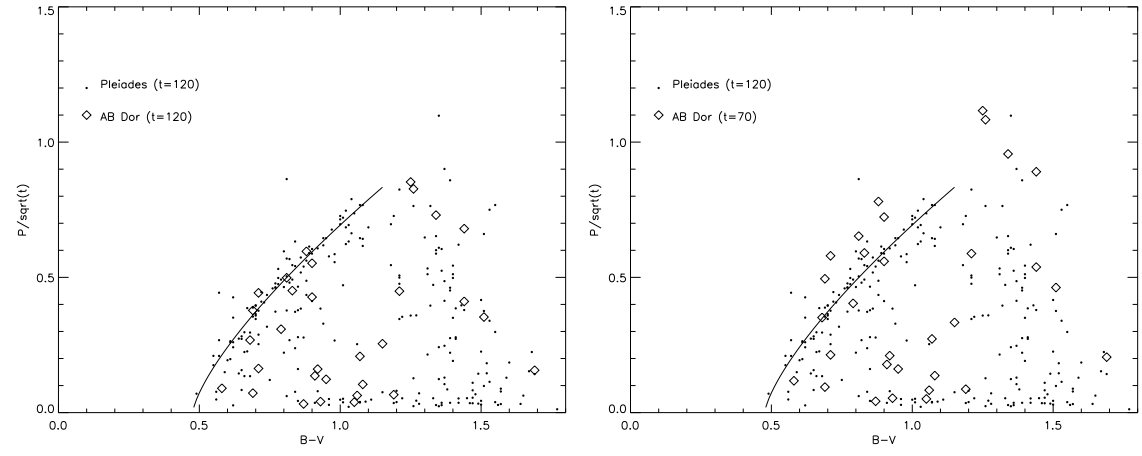

Figure 5.2: Comparison of the AB Dor rotaion periods vs. (B-V) relationship with the Pleiades. Rotation are scaled to the part of eq. 3.13 age-dependent *g(t)*. Rhombus symbols are AB Dor stars and dots are Pleiades members. In the left panel AB Dor is assumed to have the same age as the Pleiades (120 Myr). In the right panel AB Dor is assumed to have an age of 70 Myr.

The comparison of the rotational periods vs. (B-V) distribution in both cases shows an offset in the slow-rotators sequence if AB Dor is considered to be 70 Myr old. The AB Dor mean rotation periods are much closer to those predicted by the relation if stars are considered as old as the Pleiades.

5.2 Lithium abundance comparison between AB Dor and the Pleiades

Fig. 5.3 shows the comparison between the Li abundances obtained for AB Dor (rhombus symbols) and those of the Pleiades (dots symbols). With different symbols (asterics for AB Dor stars and cross for Pleiades) are represented the ultra-fast rotators ($P \leq 1.5 days$). Observations are compared to predictions of the two models made by Baraffe et al. (1998) and Allard et al. (2011) at an age of 100 Myr. The chosen of models at an age of 100 Myr has been due to limitation in temporal coverage of Baraffe et al. (1998) models, so to make the analysis coherent as much as possible have been used models at the same age (this fact will not influence the analysis because from a comparison of Allard et al. (2011) models at 100 or 120 Myr the difference in lithium abundances is negligible).

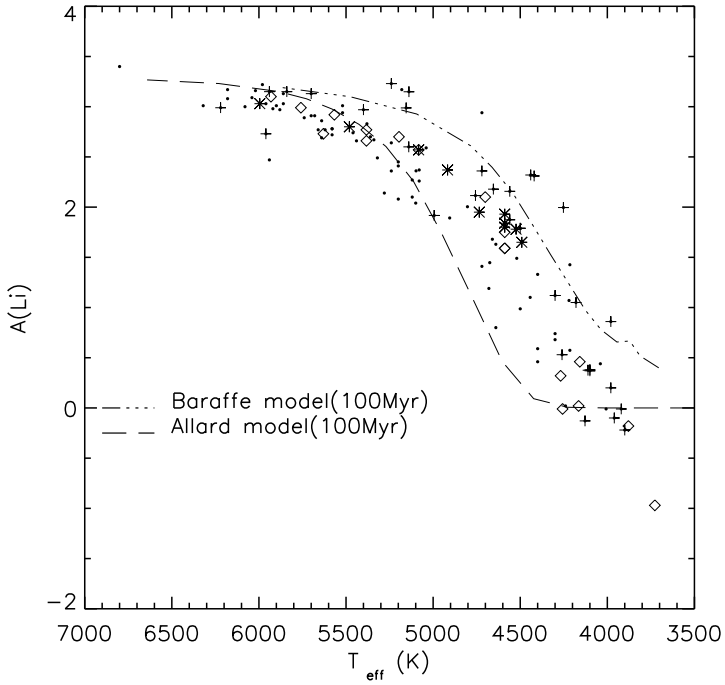

Figure 5.3: Li abundance vs. T_{eff} for the AB Dor moving group and the Pleiades cluster. Rhombus and asterics are the slow and fast rotators for AB Dor, while dots and cross symbols are slow and fast rotators for the Pleiades. Dot-dashed line is Baraffe model for 100 Myr. Long dashed line is the Allard model for 100 Myr.

The methods used for the derivation of A(Li) in the literature are different between AB Dor and the Pleiades. In the Pleiades' case Sestito et al. (2005) derived Li abundances from T_{eff} and deblended W(Li) (6708$\mathring{A}$) by interpolation of the curve of growth (COG) of Soderblom et al. (1993b). For AB Dor, da Silva et al. (2009) calculated theoretical equivalent widths of the Li lines (6708$\mathring{A}$) and compared them with

their corresponding observed values. The abundance was changed until the difference between the calculated and the observed W(Li) was smaller than $0.2m\mathring{A}$ while the other model parameters, like metallicity, surface gravity $\log g$ (4.5 for the dwarfs and 4.0 for the subgiants) and microturbolence velocity were kept fixed. Despite this, da Silva et al. (2009) found no significant difference in the A(Li) distribution vs. T_{eff} between the AB Dor association and the Pleiades.

In order to outline possible difference between AB Dor and the Pleiades, the mass-dependence of both P_{rot} and A(Li) has been removed as in Chap. 4 assuming that AB Dor has the same age as the Pleiades. Fig. 5.6 shows that, apart the $0.74 \leq (B-V) \leq 0.91$ bin when using the Allard et al. (2011) model, all AB Dor values lies very close to the Pleiades ones in the residual-P_{rot} vs. residual-A(Li) plane.

In the $0.74 \leq (B-V) \leq 0.91$ bin there is a group of 3 stars of the AB Dor association that appear Li-overabundant when adopting the Allard et al. (2011) model to remove the mass-dependence of A(Li). The difference between the results obtained by the two models is due to the fact that the A(Li) vs. T_{eff} relationships predicted have very different slopes in this range.

5.3 Lithium equivalent widths comparison between AB Dor and the Pleiades

To see how the models influence such comparison, the same analysis has been applied in the W(Li) vs. (B-V) plane. In Fig. 5.4 W(Li) vs. (B-V) of AB Dor and the Pleiades are compared. Notice that in the $0.74 \leq (B-V) \leq 0.91$ range there is a group of high W(Li) stars of AB Dor which are not UFRs. The difference in W(Li) with respect to, e.g., the Pleiades value are much larger than one could expect, for istance, from an incorrect removal of lines blended with the LiI ($6708\mathring{A}$) line.

The removal of the mass-dependence of W(Li) requires again the use of models. Unfortunately, this is possible using the Allard et al. (2011) model only, since the Baraffe et al. (1998) relationship vs. (B-V) is not available to us. The results are shown in Fig. 5.7 in which the same group of AB Dor stars with high W(Li) stands out clearly in the $0.74 \leq (B-V) \leq 0.91$ bin.

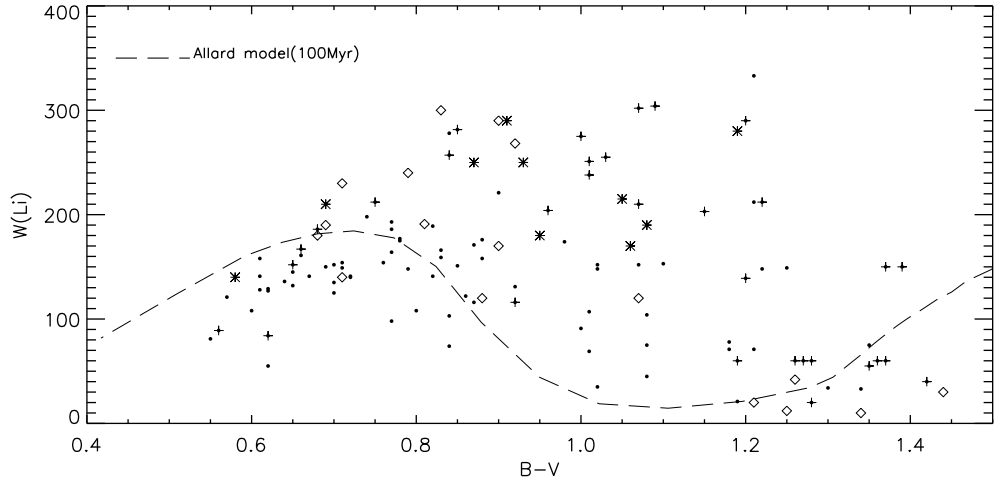

Figure 5.4: Lithium equivalent widths vs (B-V) for the AB Dor moving group (the asterics are the ultra-fast rotators) and the Pleiades cluster. Rhombus and asterics are the slow and fast rotators for AB Dor, while dots and cross symbols are slow and fast rotators for the Pleiades. Dashed line is the Allard model for 100 Myr.

5.4 Statistical analysis of the Lithium and rotation distributions

To quantify in a statistical sense the comparison of the rotation and lithium distributions in the AB Dor association and the Pleiades cluster the two-sided Kolmogorov-Smirnov (KS) test (Press et al. (2007) Cap. 14 and reference there in) has been applied (as implemented in the `KSTWO` routine in the IDLAstrolib). The KS statistics, *d*, and associated probability, *prob*, give the probability that two distributions are realisations drawn from the same distribution.

The results obtained for the P_{rot} and A(Li) observations in AB Dor and the Pleiades are shown in Fig. 5.5, where the cumulative distribution functions (CDF) are plotted, and in Tab. 5.1, where the d-statistic and prob are reported.

Table 5.1: Kolmogorov-Smirnov tests output once it's applied to period and lithium abundances distributions for AB Doradus and the Pleiades and for AB Dor simulated distribution.

	K-S real		K-S simul	
	d	prob	d	prob
Period	0.139	0.627	0.140	0.619
A(Li)	0.183	0.417	0.135	0.749

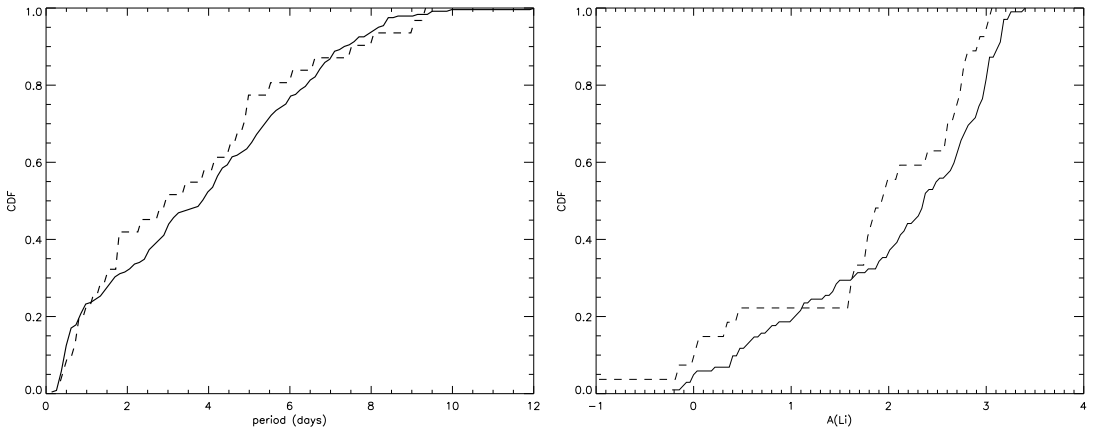

Figure 5.5: Rotation period and lithium abundance cumulative distributions for the Pleiades (solid line) and AB Dor (dashed line).

In a strict sense the KS-test gives a definitive answer when the two realisations are not drawn from the same distribution. In this respect, the results obtained support somehow the conclusions drawn so far from the qualitative comparison of the distributions.

Since the AB Dor and the Pleiades samples are very unbalanced in number, have been compared the results obtained with a simulation in which the same number of P_{rot} and A(Li) values as available for AB Dor are extracted at random from the Pleiades data. This was repeated 50 times and the mean K-S parameters obtained compared with those obtained from the real data. The results of this simulation are reported in table 5.1.

The comparison between the K-S parameters obtained from the real data and from the simulation shows that the K-S test do not disprove the assertion that the P_{rot} data of AB Dor and the Pleiades are drawn from the same distribution. The results obtained for A(Li), on the other hand, show that in this case such evidence is somewhat weaker, the probability that the two dataset are drawn from different distribution being higher. This supports somewhat quantitatively the idea that the P_{rot} distributions indicate a very similar age for the AB Dor and the Pleiades, while the A(Li) distributions point to a different scenario for the Li-depletion in the two cases. Note, however, that the A(Li) CDF of AB Dor shows a deficiency of stars between $0.5 \lesssim A(Li) \lesssim 1.6$, which may be due to incompleteness of the observed sample.

5.5 Discussion

The analysis of the rotational and Li distributions done in this chapter confirms that the AB Dor moving group is older than 70 Myr (as reported by Torres et al. (2008)) and most likely coeval with the Pleiades cluster (120 Myr old). This results are consistent with Luhman et al. (2005) and Ortega et al. (2007). The rotational periods, the Li equivalent widths and abundances of AB Dor are similar to the values observed for stars in the Pleiades. These age diagnostics are consistent with the coevality of the AB Dor group and the Pleiades. These characteristics could be added to other features (like $v \sin i$, H_α and galactic dynamics) that provided in the past years independent supporting evidence of their common origin, as said at the beginning of this chapter.

There is some evidence, however, that the stars in the two systems may have experienced somewhat different Li-depletion in their evolution. A confirmation of this proposition requires further observations, possibly from homogeneous and as complete as possible surveys. If confirmed, such differences could outline the role of the stellar environment in determins the stellar rotational hystory from which the Li-depletion appears to depend.

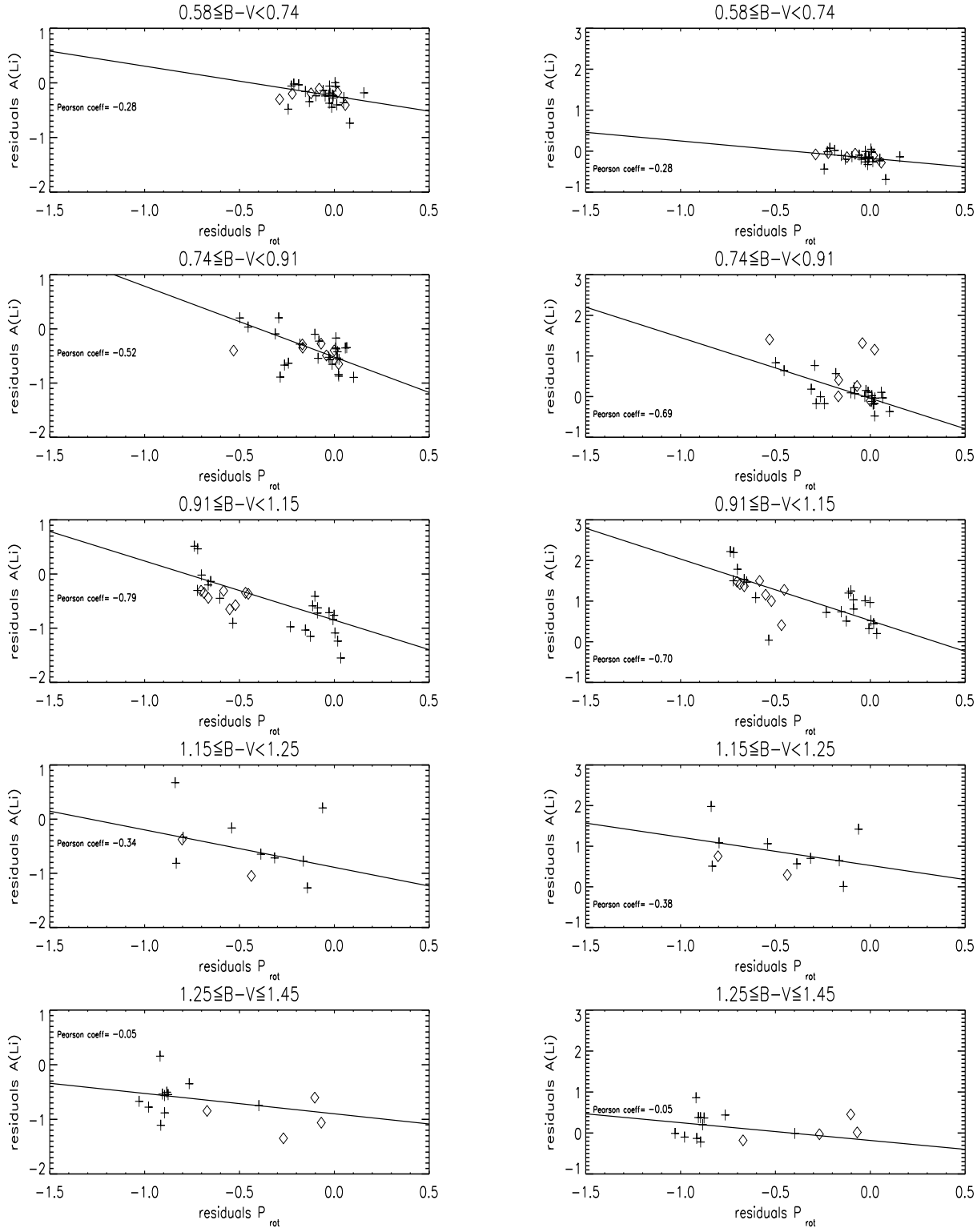

(a) Baraffe model

(b) Allard model

Figure 5.6: Residual A(Li) (from Baraffe et al. (1998) (a) and Allard et al. (2011) (b) models) as functions of residual P_{rot} $(P - P_{fit})$ for different (B-V) color bins. The cross symbols are the Pleiades while the rhombus are AB Dor stars. The Pearson coefficient is referred to Pleiades data.

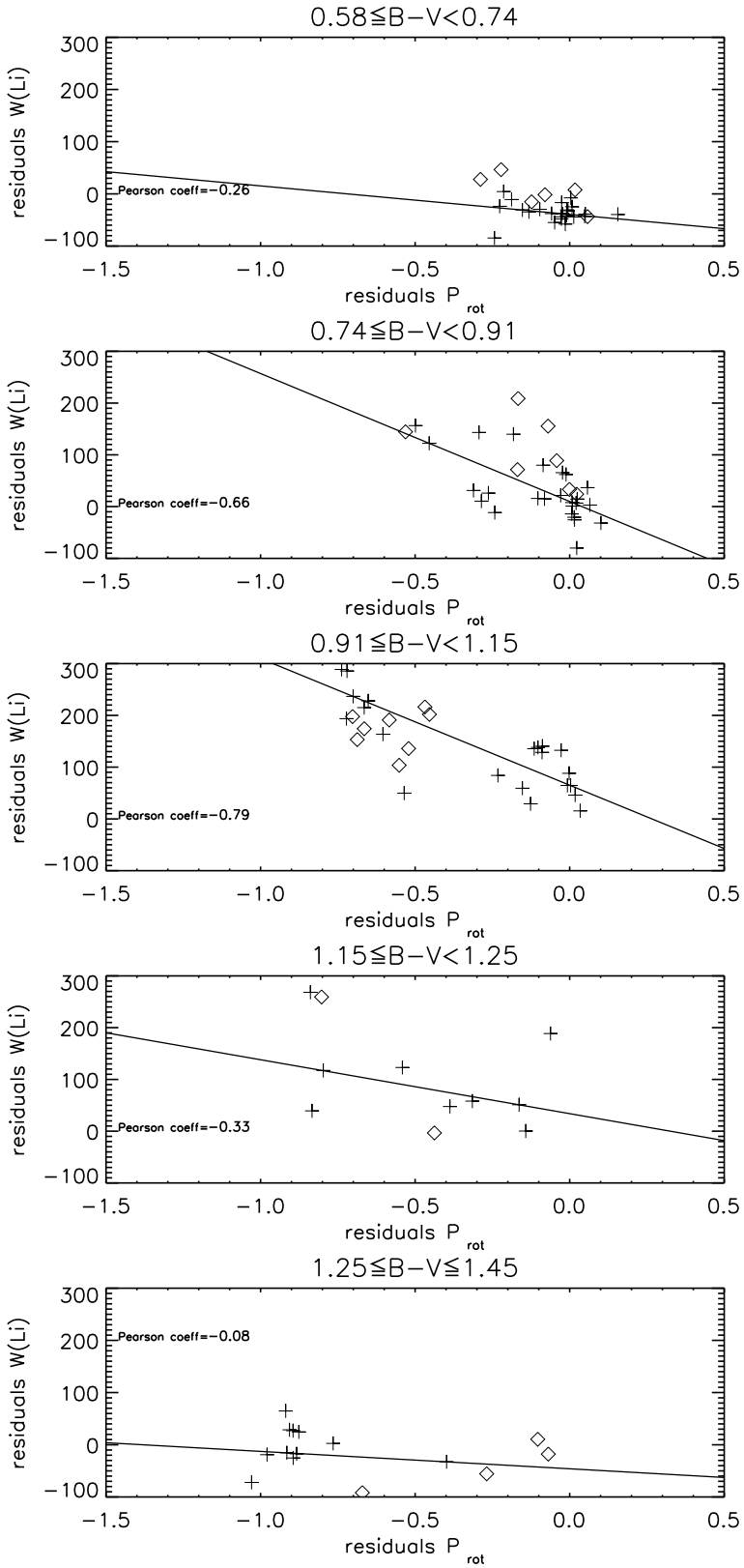

Figure 5.7: Residual lithium equivalent widths (from Allard et al. (2011) model) as functions of residual P_{rot} $(P - P_{fit})$ for different (B-V) color bins. The cross symbols are the Pleiades qhile the rhombus are AB Dor stars. The Pearson coefficient is referred to Pleiades data.

Chapter 6

Gaia-ESO Public Spectroscopic Survey: $\gamma^2 Velorum$

The Gaia-ESO Public Spectroscopic Survey (GES) (Gilmore et al. (2012)) is obtaining high quality spectroscopy of some 100000 Milky Way stars in the field and in open clusters. This ground-based survey will provide the first homogeneous overview of the distributions of kinematics and chemical elements abundances in the Galaxy with 300 nights of observations using FLAMES (both GIRAFFE and UVES) on the VLT's Unit Telescope 2 (UT2). The Gaia mission will provide photometry and astrometry of unprecedent precision for most stars and obtain low resolution spectra for most stars brighter than 17th magnitude. Gaia has limited spectroscopic capabilities, like all spacecraft, so the goal of this survey is to enlarge the amounts of information of higher quality. GES started on December 31, 2011 and will go on for 4(+1) years using 50 nights per semester.

The γVel cluster is the first young open cluster observed by this survey. A preliminary analysis of the Gaia-ESO data are presented in this chapter. $\gamma Velorum$ is a binary system consisting of the closest known Wolf-Rayet star, $\gamma^2 Velorum$, and an early high-mass O type companion, $\gamma^1 Velorum$. Several hundred pre-main sequence stars have been identified in γVel direction and that of the Vela OB2 association. Pozzo et al. (2000) found a young and exceptionally rich population of low-mass active stars that are kinematically coherent (mean radial velocity $\sim 18 kms^{-1}$) and spatially concentrated around $\gamma^2 Vel$ (RA= 08 09 31.95013, Dec= -47 20 11.710826). It is a nearby cluster for wich Gaia will give very precise proper motions and distance. It's in a critical age range ($\sim 5 - 10 Myr$), 350 pc far from the Sun and with an excellent Spitzer/X-ray coverage of the central part and good optical photometry.

6.1 Dynamical and optical analysis

The survey activities are structured into 18 Working Groups (WG). Photometry, astrometry, initial membership and general information on the cluster (like age and distance) are provided by WG1, WG2, and WG4. Raw data are reduced by WG7. Radial velocities (RV) are provided by WG8. As member of WG10, WG11 and WG12 I worked on $\gamma^2 Velorum$ spectra obtained with GIRAFFE [1] in the high resolution setup.

Despite Hernández et al. (2008) catalog contains 579 candidate members for $\gamma^2 Vel$, based on optical and NIR photometry, the final candidate members were those identified by Jeffries et al. (2009) for which are available photometric measures.

The anlysis of radial velocities (Fig. 6.1) shows that the mean radial velocity value is $\sim 18 kms^{-1}$ but it is possible to identify a signature of kinematic substructure. The presence of two different stars populations have been modelled in term of two gaussian distributions with different widths. The parameters for the expected mean central values (μ) and standard deviations (σ) are listed in the following table (Tab. 6.1):

Table 6.1: Derived values for the two gaussian distributions' parameters.

	μ	σ
Pop A	16.64	0.49
Pop B	18.26	2.62

The cluster presents two population separated by about $2 kms^{-1}$ in radial velocity. One has a broader velocity dispersion than the other. Once it has been found the presence of two possible populations it is important to search for other evidences for such kinematic substructures that might be indicative of multiple star forming events and a spread of stellar ages. Fig. 6.3 shows the spatial distribution of the stars in this sample while Fig. 6.2 shows what is the percentage of stars within a certain distance from $\gamma^2 Vel$. With red and blue colours are plotted the stars for which $RV < 18 kms^{-1}$ (Pop A) and $RV \geq 18 kms^{-1}$ (Pop B).

Despite their center is about that of $\gamma^2 Vel$ the two populations have different spa-

[1] GIRAFFE is a medium-high resolution (R=7500-300000) spectrograph for the entire visible range 370-900 nm. It is equipped with two diffraction gratings, high and low resolution. GIRAFFE is equipped with a $2K \times 4K$ EEV CCD ($15 \mu m$ pixels).

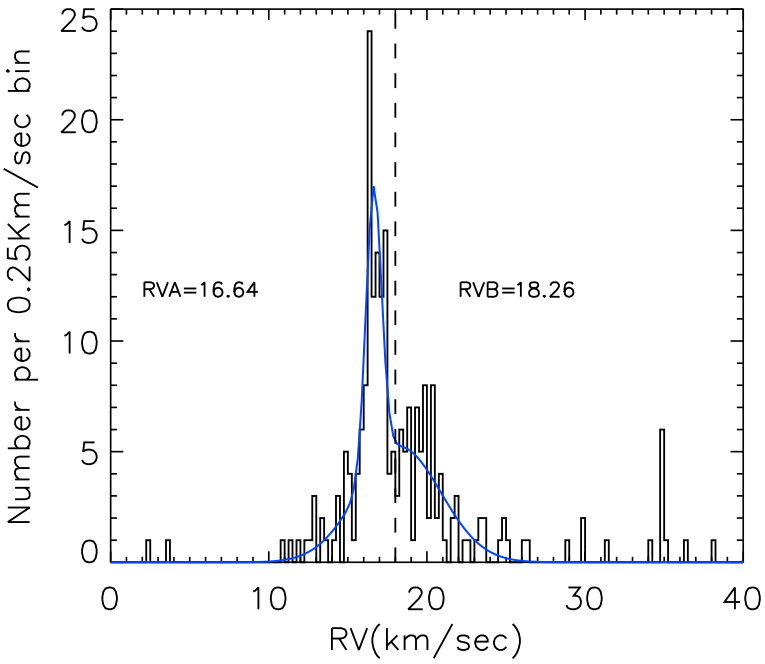

Figure 6.1: Histogram of radial velocities stars in $\gamma^2 Vel$. With blue line the function described by the sum of two gaussian distributions with the parameters reported in table 6.1.

tial distribution. It seems that Pop B stars are more dispersed across the field than those belong to Pop A, more concentrated around $\gamma^2 Vel$. Almost 40% of Pop A is 0.25 deg from the center compared with only $\sim 20\%$ of Pop B. There is also a small difference analyzing their average proper motion (Fig. 6.4). Mean values obtained are reported in Tab 6.2:

Table 6.2: Average values for the proper motions of the two populations.

	Pop A ($RV < 18 kms^{-1}$)	Pop B ($RV \geq 18 kms^{-1}$)
PM RA	-3.447	-3.898
PM Dec	9.086	7.611

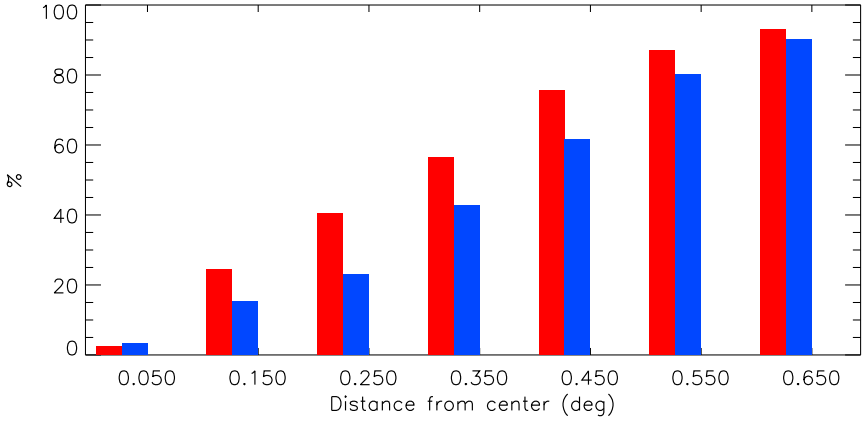

Figure 6.2: Percentage of stars in $\gamma^2 Vel$ cluster within different distances from γVel. Red color is for Pop A while blue is for Pop B.

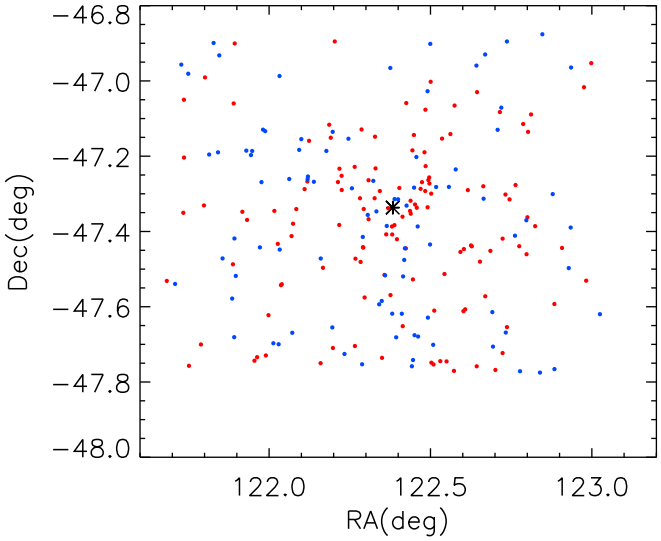

Figure 6.3: Space distribution of stars in $\gamma^2 Velorum$ cluster. With red points stars with $RV < 18 kms^{-1}$ (pop A) while blue points are those for wich $RV \geq 18 kms^{-1}$ (Pop B). Asterisk are γVel coordinates.

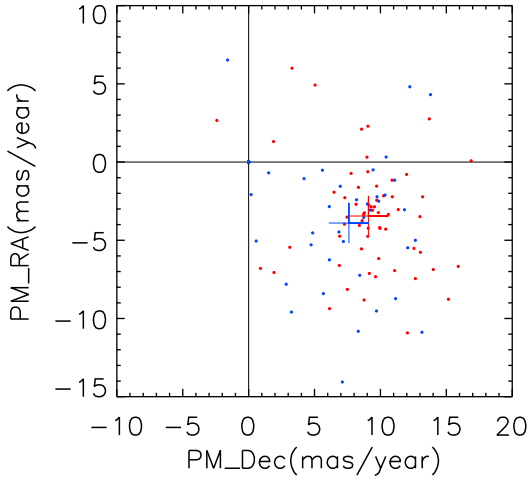

Figure 6.4: Proper motions for the two populations. With cross symbols the average proper motions. Whit red colour population with $RV < 18 kms^{-1}$ while blue colour is for that with $RV \geq 18 kms^{-1}$.

The (V-I) colour index offers many advantages. Technologically, the I-band is the reddest well-calibrated passband measurable with CCD cameras, so both V and I can be measured with the same instrument (as opposed to combining optical and near-infrared observations, wich require different instrumentation). Using photometric criteria based on the color magnitude diagram (CMD), V vs. (V-I) (Fig. 6.5), it is possible to show how the candidates of $\gamma^2 Velorum$ all lie on the same sequence. The two populations do not separate in the CMD.

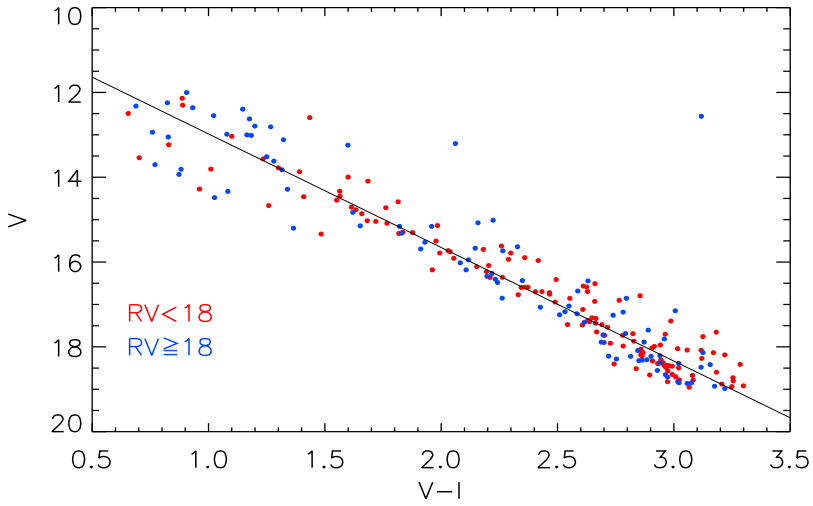

Figure 6.5: Color-magnitude diagram illustrating the selected candidates of $\gamma^2 Velorum$ cluster. Red points are stars with $RV < 18 kms^{-1}$ (Pop A) while blue points are those for wich $RV \geq 18 kms^{-1}$ (Pop B).

6.2 Lithium analysis

In Sect. 6.1 it has been found that stars around $\gamma^2 Vel$ system seems to belong to two different populations that differ partially from the dynamical point of view, but are indistinguishable in the color magnitude diagram. A further lithium analysis has been made to search possible differences in the two populations. After checking the input data, the presence of LiI absorption lines (6708$\mathring{A}$) with $W \geq 50 m\mathring{A}$ and/or $H\alpha$ emission are flagged. Lithium measurments have been carried out using the `SPLOT` task of the IRAF [2] package. The W(Li) measurements vs. RV are shown in Fig. 6.6.

The GIRAFFE spectra have been flagged to select those for which the H_α and LiI wavelength region need to be masked in the ROTFIT anlaysis, which produces $\log T$, $\log g$, $[Fe/H]$ and $v \sin i$. The ROTFIT code was developed by Frasca et al. (2003) and Frasca et al. (2006). The method used in ROTFIT consists in comparing spectra of program stars with a library of spectra of reference stars with the aim of finding several reference stars which spectra are most similar to the target spectrum. Since the program star may rotate faster than the reference, in the course of computations the latter spectrum is rotationally broadened in a wide range of velocity to find the best fit. When the most similar reference stars are found, the means of their atmospheric parameters are computed and adopted as estimates of the as-

[2]IRAF is distributed by the National Optical Astronomy Observatory, which is operated by the Association of the Universities for Research in Astronomy, inc. (AURA) under cooperative agreement with the National Science Foundation.

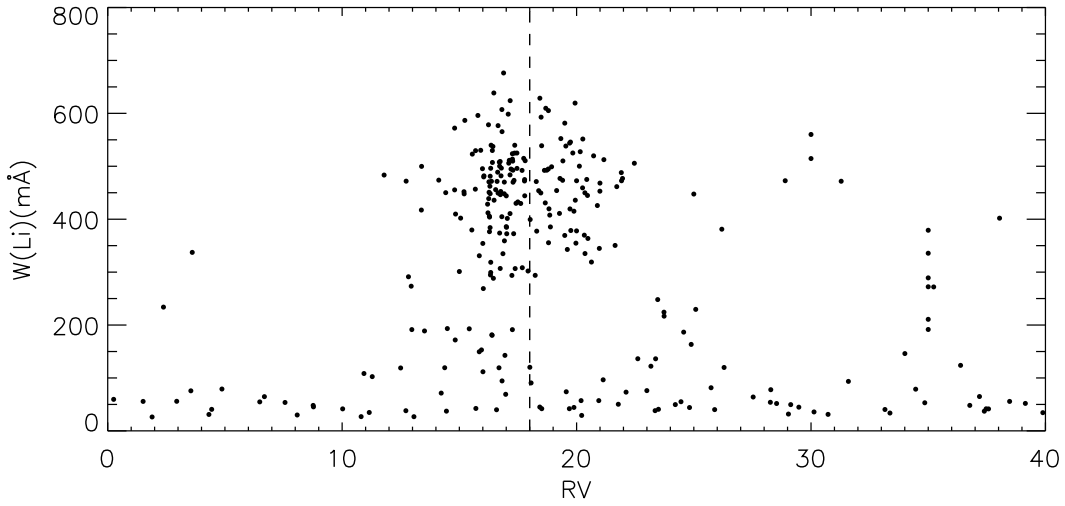

Figure 6.6: EW(Li) vs. radial velocity for all the stars selected by Jeffries et al. (2009).

trophysical parameters of the target. For the reliability of the adopted means, it is crucial that the grid of the reference spectra is sufficiently dense and homogeneous.

To derive A(Li), from the line at 6708$\mathring{A}$, the curves of growth (COGs) from Palla et al. (2007) and Soderblom et al. (1993b) have been used. The COGs from Palla et al. (2007) have been used only for cool stars ($T_{eff} < 4000K$). For warmer stars the COGs used are that from Soderblom et al. (1993b) which are calculated for T_{eff} ranging between 4000 and 6500 K. However, since the two COGs are calibrated in different T_{eff} ranges, a matching between the relationships and an interpolation in the neighborhood of 4000 K was performed. The final curves of growth are shown in Fig. 6.7.

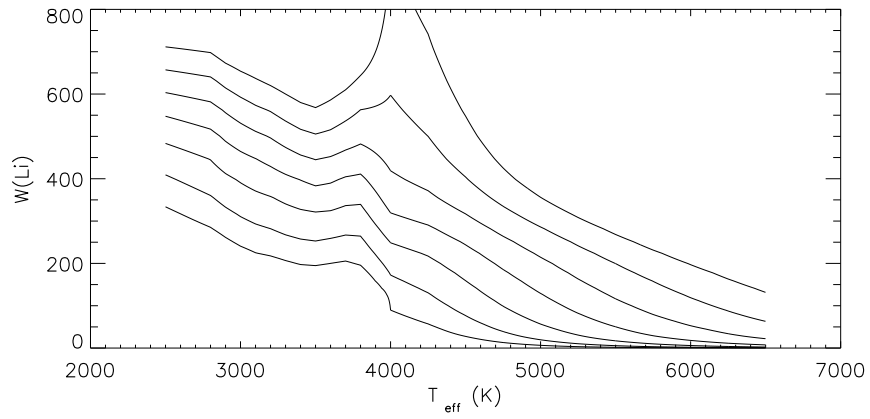

Figure 6.7: The plot shows the relation between EWs and T_{eff} at fixed Li abundance ($\log N(Li) = 0.5, 1.0, 1.5, 2.0, 2.5, 3.0, 3.5$) and $\log g = 4.5$. The final COGs is a matching and an interpolation of Palla et al. (2007) and Soderblom et al. (1993b) relations.

The models used in this analysis are those of Siess et al. (2000) and BT-Settl models by Allard et al. (2011). The lithium analysis presented here regards objects that appear to be members based on their lithium equivalent widths ($W \geq 100 m\mathring{A}$). From Fig. 6.8 it is possible notice to that the analysis in the $A(Li)$ vs. T_{eff} diagramis is not easy.

The models considered do not predict any surface Li destruction in stars hotter than $\sim 4300K$. The temperature at which is reached the maximum of depletion is different comparing the models despite the abundance is similar. Siess et al. (2000) model for 10 Myr predicts too much depletion, but none of the models reproduces the data accurately.

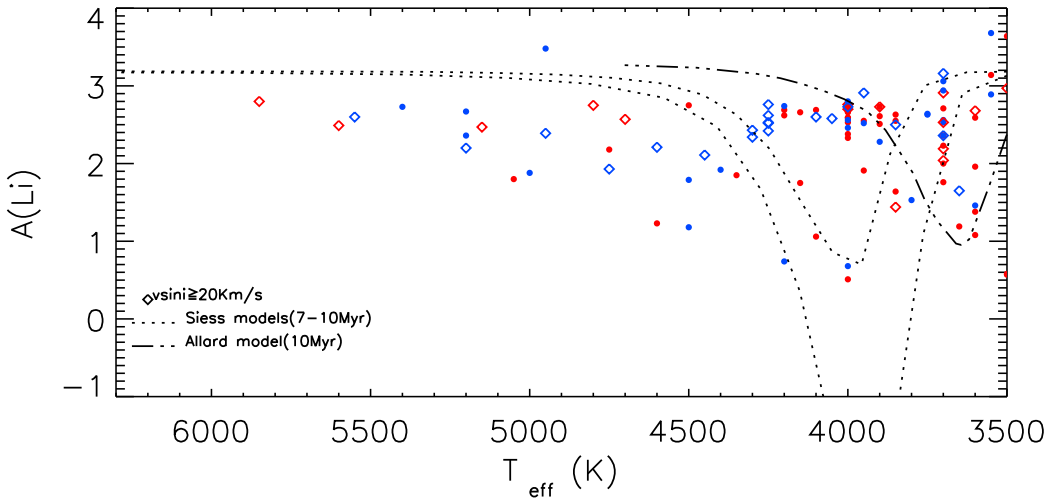

Figure 6.8: $\log N(Li)$ vs. T_{eff} for the $\gamma^2 Velorum$ cluster. Rhombus and dots symbols are fast ($v \sin i \geq 20 KMs^{-1}$) and slow rotators. Red and blue colors are for $RV < 18 kms^{-1}$ and $RV \geq 18 kms^{-1}$. Dotted lines are Siess et al. (2000) models for 7 and 10 Myr. Dot-dashed line is the Allard et al. (2011) model for 10 Myr.

Moving to a A(Li) vs. (V-I) diagram and separating the general behavior from that of fast rotator ($v \sin i \geq 20 KMs^{-1}$) Fig. 6.9 and Fig. 6.10 are obtained.

The 7 Myr Siess et al. (2000) model does not reproduce the observed lithium depletion trend. The slope in the 20 Myr Allard et al. (2011) model reproduces vaguely that of observations. No clear differences are evident between the two populations if not a small group of Pop A stars with $2.6 < (V - I) < 2.7$ that shows a lower lithium abundance value ($\sim 0.5 dex$). It seems that for (V-I) higher than ~ 2.3 Pop A and Pop B stars follow whitout distinction the curve at 10 Myr and at 20 Myr. Identical behavior, even making use of fundamental stellar properties such as equivalent width and (V-I) color, as shown in Fig. 6.11 and Fig. 6.12.

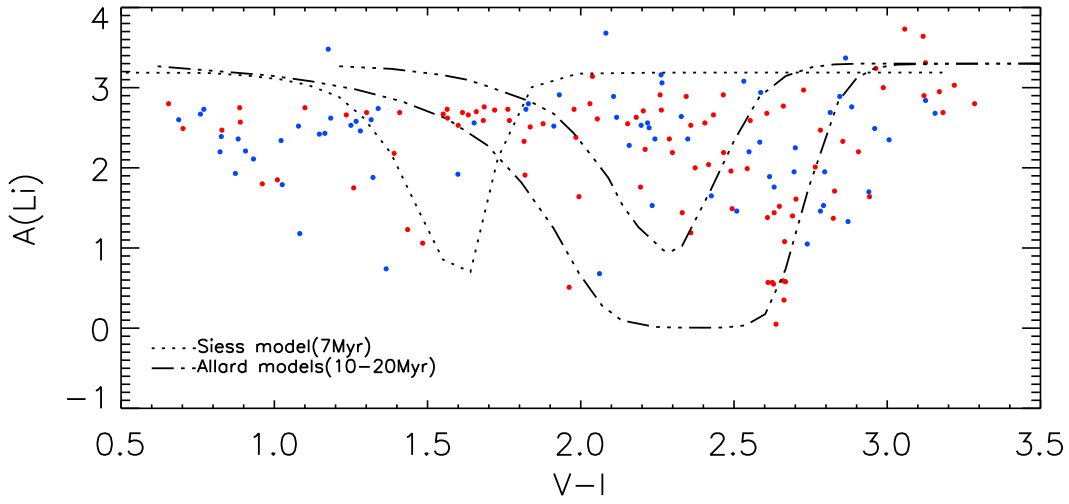

Figure 6.9: A(Li) vs. (V-I) for the $\gamma^2 Velorum$ cluster. Red and blue colors are for $RV < 18 kms^{-1}$(Pop A) and $RV \geq 18 kms^{-1}$ (Pop B). Dotted lines is Siess et al. (2000) model for 7 Myr. Dot-dashed line are the Allard et al. (2011) models for 10 and 20 Myr.

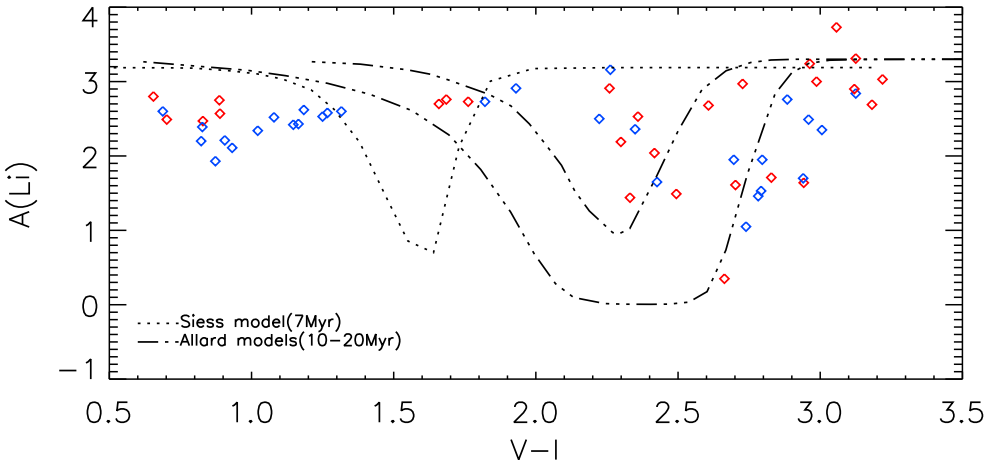

Figure 6.10: A(Li) vs. (V-I) for the $\gamma^2 Velorum$ fast rotators ($v \sin i \geq 20 KMs^{-1}$). Red and blue colors are for $RV < 18 kms^{-1}$ (Pop A) and $RV \geq 18 kms^{-1}$ (Pop B). Dotted lines is Siess et al. (2000) model for 7 Myr. Dot-dashed line are the Allard et al. (2011) models for 10 and 20 Myr.

The discussion can be closed saying that:

- $\gamma^2 Velorum$ cluster shows kinematic substructure with evidence for 2 populations: Pop A (with $RV < 18 kms^{-1}$) and Pop B (with $RV \geq 18 kms^{-1}$);
- Pop B has a large velocity dispersion ($\sim 2.62 kms^{-1}$);
- Pop A has a very small velocity dispersion ($\sim 0.49 kms^{-1}$) and is centrally concentrated around $\gamma^2 Vel$ Wolf-Rayet star;

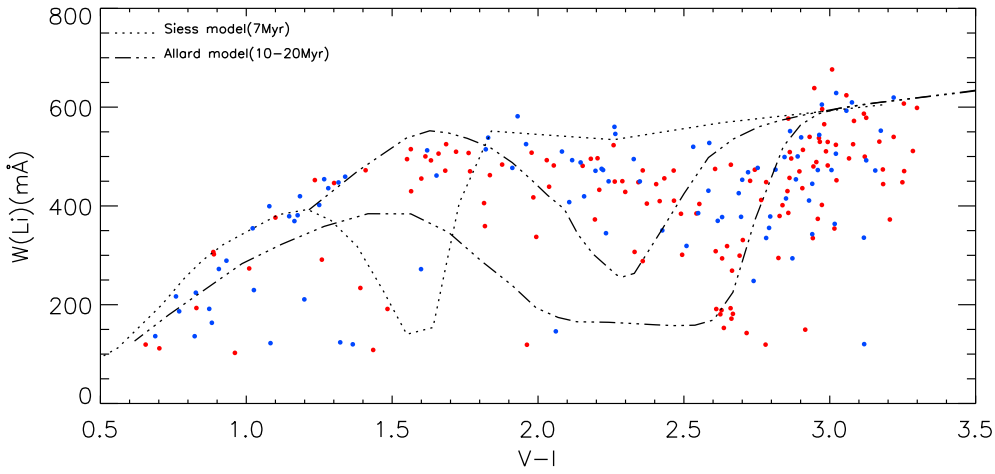

Figure 6.11: EW(Li) vs. (V-I) for the $\gamma^2 Velorum$ cluster. Red and blue colors are for $RV < 18 kms^{-1}$ (Pop A) and $RV \geq 18 kms^{-1}$ (Pop B). Dotted lines is Siess et al. (2000) model for 7 Myr. Dot-dashed line are the Allard et al. (2011) models for 10 and 20 Myr.

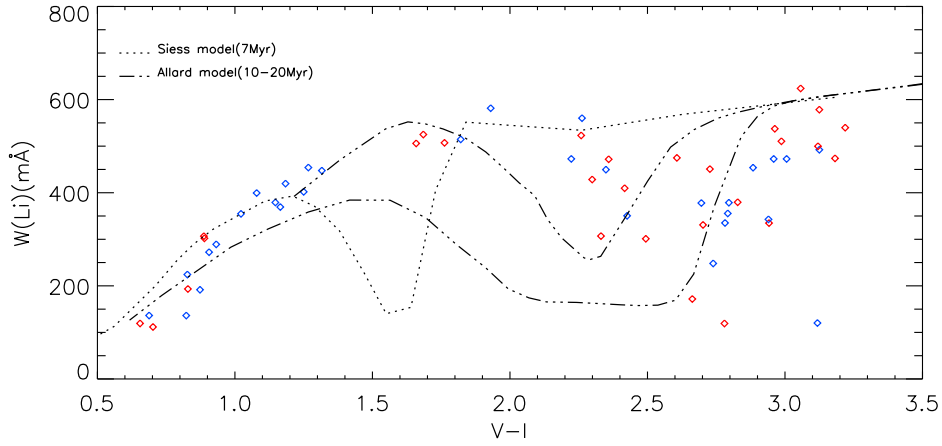

Figure 6.12: EW(Li) vs. (V-I) for the $\gamma^2 Velorum$ fast rotators ($v \sin i \geq 20 KMs^{-1}$). Red and blue colors are for $RV < 18 kms^{-1}$ (Pop A) and $RV \geq 18 kms^{-1}$ (Pop B). Dotted lines is Siess et al. (2000) model for 7 Myr. Dot-dashed line are the Allard et al. (2011) models for 10 and 20 Myr.

- on CMD diagram the two populations lie on the same sequence;
- the poor fit of the lithium data to the models leads to rather large uncertainties on the ages, the amount of lithim depletion is more congruent with Allard et al. (2011) model at 20 Myr;
- despite the disagreement between model's age and that found by Jeffries et al. (2009), it has not been observed a difference, however small, between the lithium in the two populations.

Chapter 7

Conclusions

The exsistence of spreads in rotation rates and lithium abundances among a group of stars of about the same age, that models still can not reproduce, emphasize how poorly we understand those phenomena that are so central for the evolution of solar-type stars. Stars in open clusters form samples that are complete in mass and homogeneous in environmental conditions, initial chemical composition and age. These stars are the best sample to investigate the dependence on age of rotational period. The knowledge of rotational periods allow to investigate the effects of rotation on the lithium depletion and to establish if it is present a connection between them.

Yet, stellar ages are critical to establish. The use of rotation as a clock is useful if it is competitive with other techniques for determining ages. Ages may be determined by comparing a star's location on the CMD to stellar model prediction (if the distance and metal content is known). Without helium or metallicity information stellar isochrones suffer a degeneracy with age. Another technique is asteroseismology that obtains age estimates for dwarfs by measuring the helium content. It's good to 10% of a star's main sequence lifetime, making the best age constraints possible for more massive stars. In the low mass regime, however, stellar pulsation may not even be detectable. As noticed by Epstein et al. (2012) both measure ages are based on changes on the nuclear timescale and suffer higher uncertainties for low mass stars. In comparison rotation-mass-age relationships are not competitive for stars more massive than the Sun, but in an intermediate mass regime are clearly the best possible age indicators available.

In this work a relationship that correlates to age the rotation period data currently available for solar- and late-type stars in 9 observed open clusters with ages between

120 Myr and 1 Gyr has been proposed. The progressive evolution of the morphology with age suggests that color-period diagrams, although harder to construct, could be used in similar ways to color-magnitude diagrams, especially for young open clusters, for age determination. It has been showed how the slow rotators sequences of all clusters cannot be described using only one curve parameterized by age and (B-V) color. The different behaviour, noticed if are considered clusters with ages $\leq 500Myr$ or older, has so been fitted considering two additional factors.

The discrepancies between the theory of stellar wind described by Kawaler (1988) and the observed rotation periods of solar and subsolar-mass stars in clusters older than $\sim 120Myr$ suggest that one or more assumptions are wrong. In particulary, it may be necessary to improve the internal angular moentum transport description, or to revise the assumed wind model. Regarding the last point, a number of new models on the origin and evolution of stellar angular momentum have been proposed in recent years by different authors. I reserve for the future the aim to work on a rotational clock that takes into account the new formulation for angular momentum evolution recently proposed by Reiners et al. (2012) and Gallet et al. (2013).

The large dispersion observed in lithium abundances at fixed temperature in cool Pleiades is a challenge for stellar evolution because standard models of uniform age and abundance are unable to reproduce it. The scatter grows with decreasing mass, $M \lesssim 0.9M_{\odot}$ and it is known, from past works, that also rotation plays a role in this spread observed. With the study presented here has been found that rotation not only influences lithium abundance but it's also correlates with it expecially in $0.74 \leq (B-V) \leq 1.15$ color range, where there is an almost one-to-one mapping. The slower the star the more lithium destroys. Rapid rotators somehow enables the stars to preserve more of their initial Li. Distinguishing specific mechanisms and their relative importance for Li depletion and scatter at a given age will require continuing observational and theoretical efforts. On the observational front, continued observations of Li in a variety of clusters spanning a range and metallicity are so needed.

The new period-mass-age relationships found in this work and the analysis on lithium depletion have been used to study the young loose association AB Doradus. Since the age estimate of AB Doradus is still argued, a comparison with the Pleiades has been used to give an estimate based on rotation. A comparison between period-(B-

V) and Li-(B-V) relationships for the Pleiades and AB Dor associations has been done. In addition the Kolmogorov-Smirnov test to these distributions has been applied. The results confirm the proposition that the AB Dor association is older than 70 Myr (Torres et al. (2008)) and coeval with the Pleiades cluster (120 Myr).

Another young cluster studied was $\gamma^2 Velorum$, thanks to the collaboration in the Gaia-ESO Public Spectroscopic Survey. The analysis of spectra has revealed two kinematic substructure for which the Li distribution is essentially undistinguishable.

7.1 Future perspectives

The research plan in the next future involves the following topics:

- take into account more recent formulation for angular momentum evolution in order to search for an unique period-mass relationship that reproduces the observed data for open clusters and predicts with enough accuracy the rotational periods of the Sun;
- the amount of new data to analyze that is providing GES and the first results obtained encourage me, even more, to give a contribution to such important project.

Bibliography

Adams, J. D., Stauffer, J. R., Monet, D. G., Skrutskie, M. F., & Beichman, C. A., *The Mass and Structure of the Pleiades Star Cluster from 2MASS*, 2001, AJ, 121, 2053

Allard, F., Homeier, D., & Freytag, B. , *Model Atmospheres From Very Low Mass Stars to Brown Dwarfs*, 2011, 16th Cambridge Workshop on Cool Stars, Stellar Systems, and the Sun, 448, 91

Archinal, B. A., & Hynes, S. J. , *Star clusters*, 2003, Star clusters; foreword by David H. Levy. Richmond, VA : Willmann-Bell,2003

Baraffe, I., Chabrier, G., Allard, F., & Hauschildt, P. H., *Evolutionary models for solar metallicity low-mass stars: mass-magnitude relationships and color-magnitude diagrams*, 1998, A&A, 337, 403

Barnes, S. A. , *On the Rotational Evolution of Solar- and Late-Type Stars, Its Magnetic Origins, and the Possibility of Stellar Gyrochronology*, 2003, ApJ, 586, 464

Barnes, S. A. , *Ages for Illustrative Field Stars Using Gyrochronology: Viability, Limitations, and Errors*, 2007, ApJ, 669, 1167

Barnes, S. A., & Kim, Y.-C. , *Angular Momentum Loss from Cool Stars: An Empirical Expression and Connection to Stellar Activity*, 2010, ApJ, 721, 675

Bell, C. P. M, Naylor, T., Mayne, N. J., Jeffries, R. D., & Littlefair, S. P. , *Pre-main sequence isochrones-I. The Pleiades benchmark*, 2012, MNRAS, 424, 3178

Bodenheimer, P. , *Studies in Stellar Evolution. II. Lithium Depletion during the Pre-Main Contraction.*, 1965, ApJ, 142, 451

Bouvier, J. , *Lithium depletion and the rotational history of exoplanet host stars*, 2008, AAp, 489, L53

Bragaglia, A. , *The Open Clusters in the Gaia-ESO Survey*, 2012, Science from the Next Generation Imaging and Spectroscopic Surveys, 3P

Butler, R. P., Marcy, G. W., Cohen, R. D., & Duncan, D. K. , *The Pleiades rapid rotators - Evidence for an evolutionary sequence*, 1987, ApJL, 319, L19

Chaboyer, B., Demarque, P., & Pinsonneault, M. H. , *Stellar models with microscopic diffusion and rotational mixing. II. Application to open clusters*, 1995, ApJ, 441, 876

Collier Cameron, A., et al. , *The main-sequence rotation-colour relation in the Coma Berenices open cluster*, 2009, MNRAS, 400, 451

Cox, A. N. , *Allen's astrophysical quantities*, 2000, Allen's Astrophysical Quantities,

Cranmer, S. R., & Saar, S. H. , *Testing a Predictive Theoretical Model for the Mass Loss Rates of Cool Stars*, 2011, ApJ, 741, 54

Dantona, F., & Mazzitelli, I. , *Lithium depletion in stars - Pre-main sequence burning and extra-mixing*, 1984, AAp, 138, 431

Danziger, I. J., & Conti, P. S. , *Lithium Observations in the Pleiades and in F Stars in the Field*, 1966, ApJ, 146, 392

D'Antona, F., & Montalbán, J. , *Efficiency of convection and Pre-Main Sequence lithium depletion*, 2003, AAp, 412, 213

da Silva, L., Torres, C. A. O., de La Reza, R., Quast, G. R., Melo, C. H. F., & Sterzik, M. F. , *Search for associations containing young stars (SACY). III. Ages and Li abundances*, 2009, AAp, 508, 833

Delorme, P., Collier Cameron, A., Hebb, L., Rostron, J., Lister, T. A., Norton, A. J., Pollacco, D., & West, R. G. , *Stellar rotation in the Hyades and Praesepe: gyrochronology and braking timescale*, 2010, SF2A-2010: Proceedings of the Annual meeting of the French Society of Astronomy and Astrophysics, 243

Denissenkov, P. A., Pinsonneault, M., Terndrup, D. M., & Newsham, G. , *Angular Momentum Transport in Solar-type stars: testing the timescale for core-envelope coupling*, 2010, ApJ, 716, 1269

Duncan, D. K. , *Rotation of young solar-type stars in the Orion Nebula region*, 1993, ApJ, 406, 172

Durney, B. R., & Latour, J. , *On the angular momentum loss of late-type stars*, 1978, Geophysical and Astrophysical Fluid Dynamics, 9, 241

Epstein, C. R., & Pinsonneault, M. H. , *How Good of a Clock is Rotation? The Stellar Rotation-Mass-Age Relationship for Old Field Stars*, 2012, arXiv:1203.1618

Frasca, A., Alcalá, J. M., Covino, E., Catalano, S., Marilli, E., & Paladino, R. , *Further identification of ROSAT all-sky survey sources in Orion*,

Frasca, A., Guillout, P., Marilli, E., Freire Ferrero, R., Biazzo, K., & Klutsch, A. , *Newly discovered active binaries in the RasTyc sample of stellar X-ray sources. I. Orbital and physical parameters of six new binaries*, 2006, AAp, 454, 301

Gallet, F., & Bouvier, J. , *Improved angular momentum evolution model for solar-like stars*, 2013, AAp, 556, A36

Garmany, C. D. , *OB associations: Massive stars in context*, 1994, PASP, 106, 25

Gilmore, G., et al. , *The Gaia-ESO Public Spectroscopic Survey*, 2012, The Messenger, 147, 25

Hartman, J. D., et al. , *Deep MMT Transit Survey of the Open Cluster M37. III. Stellar Rotation at 550 Myr*, 2009, ApJ, 691, 342

Hartman, J. D., Bakos, G. Á., Kovács, G., & Noyes, R. W. , *A large sample of photometric rotation periods for FGK Pleiades stars*, 2010, MNRAS, 408, 475

Herbig, G. H. , *The properties and problems of T Tauri stars and related objects.*, 1962, Advances in Astronomy and Astrophysics, 1, 47

Hernández, J., Hartmann, L., Calvet, N., Jeffries, R. D., Gutermuth, R., Muzerolle, J., & Stauffer, J. , *A Spitzer View of Protoplanetary Disks in the γ Velorum Cluster*, 2008, ApJ, 686, 1195

Hillenbrand, L. A. , *Age-related observations of low mass pre-main and young main sequence stars*, 2009, IAU Symposium, 258, 81

Janes, K. A., Tilley, C., & Lynga, G. , *Properties of the open cluster system*, 1988, AJ, 95, 771

Janes, K. A., & Hoq, S. , *A Quantitative Analysis of Distant Open Clusters*, 2011, AJ, 141, 92

Jeffries, R. D., Naylor, T., Walter, F. M., Pozzo, M. P., & Devey, C. R. , *The stellar association around Gamma Velorum and its relationship with Vela OB2*, 2009, MNRAS, 393, 538

Jester, S., et al. , *The Sloan Digital Sky Survey View of the Palomar-Green Bright Quasar Survey*, 2005, AJ, 130, 873

Kalirai, J. S., Ventura, P., Richer, H. B., Fahlman, G. G., Durrell, P. R., D'Antona, F., & Marconi, G. , *The CFHT Open Star Cluster Survey. III. The White Dwarf Cooling Age of the Rich Open Star Cluster NGC 2099 (M37)*, 2001, AJ, 122, 3239

Kawaler, S. D. , *Angular momentum loss in low-mass stars*, 1988, ApJ, 333, 236

King, J. R., Schuler, S. C., Hobbs, L. M., & Pinsonneault, M. H. , *Li I and KI Scatter in Cool Pleiades Dwarfs*, 2010, ApJ, 710, 1610

Luhman, K. L., Stauffer, J. R., & Mamajek, E. E. , *The Age of AB Doradus*, 2005, ApJL, 628, L69

Mamajek, E. E., & Hillenbrand, L. A. , *Improved Age Estimation for Solar-Type Dwarfs Using Activity-Rotation Diagnostics*, 2008, ApJ, 687, 1264

Marquardt, W. D. , *An Algorithm for Least-Squares Estimation of Nonlinear Parameters*, 1963, J. Soc. Ind. Appl. Math., Vol 11, no. 2, 431

Matt, S. P., MacGregor, K. B., Pinsonneault, M. H., & Greene, T. P. , *Magnetic Braking Formulation for Sun-like Stars: Dependence on Dipole Field Strength and Rotation Rate*, 2012, ApJL, 754, L26

Meibom, S., Mathieu, R. D., & Stassun, K. G. , *Stellar Rotation in M35: Mass-Period Relations, Spin-Down Rates, and Gyrochronology*, 2009, ApJ, 695, 679M

Meibom, S., Mathieu, R. D., Stassun, K. G., Liebesny, P., & Saar, S. H. , *The Color-period Diagram and Stellar Rotational Evolution-New Rotation Period Measurements in the Open Cluster M34*, 2011, ApJ, 733, 115

Meibom, S., et al. , *The Kepler Cluster Study: Stellar Rotation in NGC 6811*, 2011, ApJL, 733, L9

Messina, S., Desidera, S., Turatto, M., Lanzafame, A. C., & Guinan, E. F. , *RACE-OC project: Rotation and variability of young stellar associations within 100 pc*, 2010, AAp, 520, A15

Messina, S., Parihar, P., Koo, J.-R., Kim, S.-L., Rey, S.-C., & Lee, C.-U. , *RACE-OC project: rotation and variability in the open cluster M 11 (NGC 6705)*, 2010, AAp, 513, A29

Mills, E. A., Deliyannis, C. P., Sarajedini, A., & Platais, I. , *WIYN Open Cluster Study: Further UBVRI Photometry of Hyades-Aged Open Cluster NGC 6811*, 2005, Bulletin of the American Astronomical Society, 37, 1278

Ortega, V. G., Jilinski, E., de La Reza, R., & Bazzanella, B. , *On the common origin of the AB Doradus moving group and the Pleiades cluster*, 2007, MNRAS, 377, 441

Palla, F., Randich, S., Pavlenko, Y. V., Flaccomio, E., & Pallavicini, R. , *Old Stars in Young Clusters: Lithium-depleted Low-Mass Stars of the Orion Nebula Cluster*, 2007, ApJL, 659, L41

Pinsonneault, M. H., Kawaler, S. D., Sofia, S., & Demarque, P. , *Evolutionary models of the rotating sun*, 1989, ApJ, 338, 424

Pinsonneault, M. H. , *Rotational mixing and Lithium depletion*, 2010, IAU Symposium, 268, 375

Pozzo, M., Jeffries, R. D., Naylor, T., Totten, E. J., Harmer, S., & Kenyon, M. , *The discovery of a low-mass, pre-main-sequence stellar association around γ Velorum*, 2000, MNRAS, 313, L23

Press, W. H, Teukolsky, S. A., Vetterling, W. T., & Flannery, B. P. , *Numerical Recipes, The Art of Scientific Computing*, 2007, Cambridge University Press, 2nd Edition

Radick, R. R, Thompson, D. T., Lockwood, G. W., Duncan, D. K., & Baggett, W. E. , *The activity, variability, and rotation of lower main-sequence Hyades stars*, 1987, ApJ, 321, 459

Randich, S. , *The Gaia-ESO Survey*, 2012, Chemical Evolution of the Milky Way,

Reiners, A., & Mohanty, S. , *Radius-dependent Angular Momentum Evolution in Low-mass Stars. I*, 2012, ApJ, 746, 43

Schulz, N. S. , *From Dust To Stars Studies of the Formation and Early Evolution of Stars*, 2005, Springer-Praxis books in astrophysics and astronomy

Siess, L., Dufour, E., & Forestini, M. , *An internet server for pre-main sequence tracks of low- and intermediate-mass stars*, 2000, A&A, 358, 593

Sestito, P., & Randich, S. , *Time scales of Li evolution: a homogeneous analysis of open clusters from ZAMS to late-MS*, 2005, AAp, 442, 615

Skumanich, A. , *Time Scales for CA II Emission Decay, Rotational Braking, and Lithium Depletion*, 1972, ApJ, 171, 565

Soderblom, D. R., Stauffer, J. R., MacGregor, K. B., & Jones, B. F. , *The evolution of angular momentum among zero-age main-sequence solar-type stars*, 1993, ApJ, 409, 624

Soderblom, D. R., Jones, B. F., Balachandran, S., Stauffer, J. R., Duncan, D. K., Fedele, S. B., & Hudon, J. D. , *The evolution of the lithium abundances of solar-type stars. III - The Pleiades*, 1993, AJ, 106, 1059

Soderblom, D. R., Nelan, E., Benedict, G. F., McArthur, B., Ramirez, I., Spiesman, W., & Jones, B. F. , *Confirmation of Errors in Hipparcos Parallaxes from Hubble Space Telescope Fine Guidance Sensor Astrometry of the Pleiades*, 2005, AJ, 129, 1616

Soderblom, D. R. , *The Ages of Stars*, 2010, ARA&A, 48, 581

Spada, F., Lanzafame, A. C., Lanza, A. F., Messina, S., & Collier Cameron, A. , *Modelling the rotational evolution of solar-like stars: the rotational coupling time-scale*, 2011, MNRAS, 416, 447

Stahler, S. W., & Palla, F. , *The Formation of Stars*, 2005, pp. 865, Wiley-VCH , January 2005.

Stauffer, J. R., Schultz, G., & Kirkapatrick, J. D. *Keck Spectra of Pleiades Brown Dwarf Candidates and Precise Determination of the Lithium Depletion Edge in the Pleiades*, 1998, ApJL, 499, L199

Stauffer, J. R., et al. , *Near- and Mid-Infrared Photometry of the Pleiades and a New List of Substellar Candidate Members*, 2007, ApJSS, 172, 663

Sung, H., Bessell, M. S., Lee, H.-W., Kang, Y. H., & Lee, S.-W. , *UBVI CCD photometry of M11 - II. New photometry and surface density profiles*, 1999, MNRAS, 310, 982

Torres, C. A. O., Quast, G. R., Melo, C. H. F., & Sterzik, M. F. , *Young Nearby Loose Associations*, 2008, Handbook of Star Forming Regions, Volume II, 757

Ventura, P., Zeppieri, A., Mazzitelli, I., & D'Antona, F., *Pre-main sequence Lithium burning: the quest for a new structural parameter*, 1998, AAp, 331, 1011

Xiong, D.-R., & Deng, L.-C., *A re-examination of the dispersion of lithium abundance of Pleiades member stars*, 2006, CAA, 30, 24

Yi, S., Demarque, P., Kim, Y.-C., Lee, Y.-W., Ree, C. H., Lejeune, T., & Barnes, S. , *Toward Better Age Estimates for Stellar Populations: The Y¡SUP¿2¡/SUP¿ Isochrones for Solar Mixture*, 2001, ApJSS, 136, 417

Zuckerman, B., Song, I., & Bessell, M. S. , *The AB Doradus Moving Group*, 2004, ApJL, 613, L65